iScience

CellPress
OPEN ACCESS

Article

RACK1 promotes *Shigella flexneri* actin-mediated invasion, motility, and cell-to-cell spreading

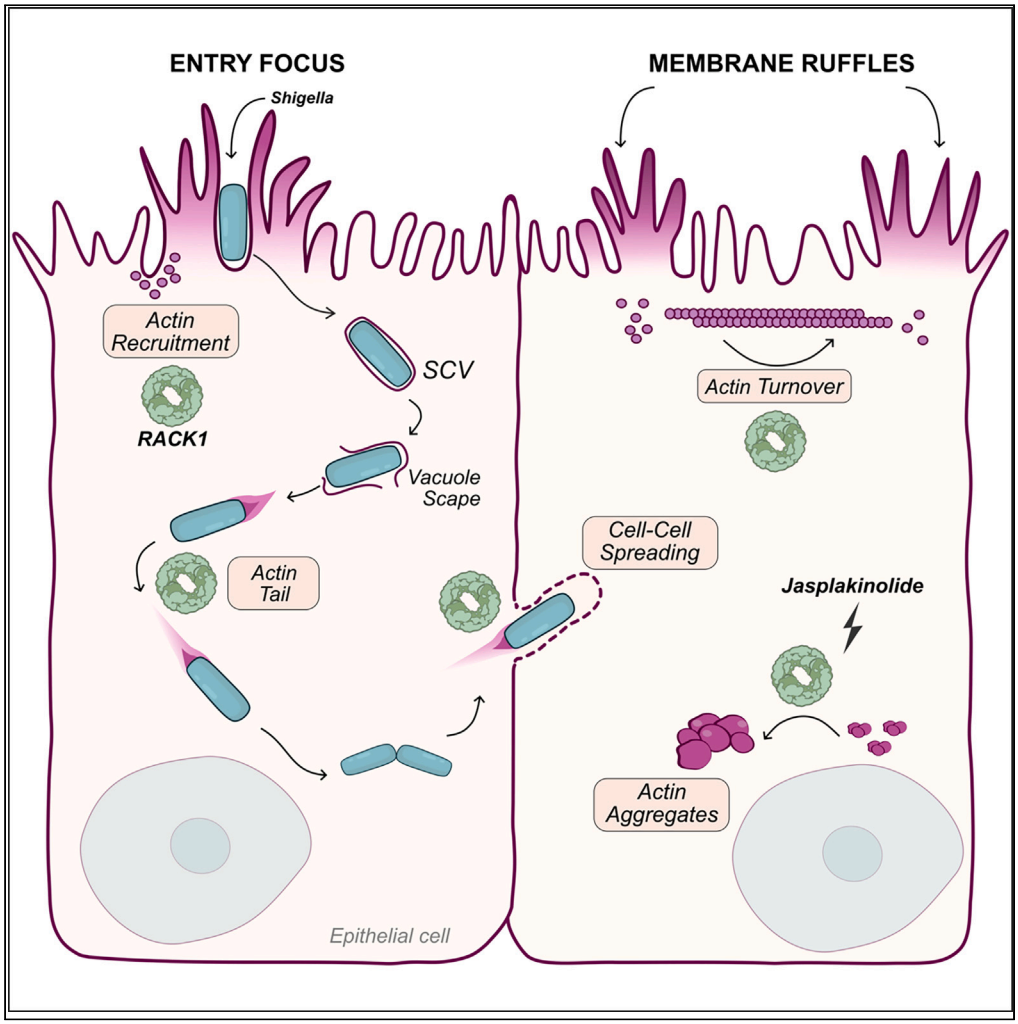

Karla N. Valenzuela-Valderas, Elmira Farrashzadeh, Yuen-Yan Chang, ..., John R. Rohde, Jost Enninga, Zhenyu Cheng

zhenyu.cheng@dal.ca

Highlights

RACK1 promotes *Shigella* growth in epithelial cells via cytoskeleton remodeling

RACK1 silencing reduces bacterial invasion, actin-mediated motility, and spreading

RACK1 promotes actin turnover and jasplakinolide-mediated actin aggregate formation

Valenzuela-Valderas et al., iScience *26*, 108216
November 17, 2023
https://doi.org/10.1016/j.isci.2023.108216

iScience

CellPress
OPEN ACCESS

Article

RACK1 promotes *Shigella flexneri* actin-mediated invasion, motility, and cell-to-cell spreading

Karla N. Valenzuela-Valderas,[1] Elmira Farrashzadeh,[1] Yuen-Yan Chang,[2,4] Yunnuo Shi,[1] Renee Raudonis,[1] Brendan M. Leung,[3] John R. Rohde,[1] Jost Enninga,[2] and Zhenyu Cheng[1,5,*]

SUMMARY

***Shigella flexneri* is an intracellular bacterium that hijacks the host actin cytoskeleton to invade and disseminate within the colonic epithelium. *Shigella*'s virulence factors induce actin polymerization, leading to bacterial uptake, actin tail formation, actin-mediated motility, and cell-to-cell spreading. Many host factors involved in the *Shigella*-prompted actin rearrangements remain elusive. Here, we studied the role of a host protein receptor for activated C kinase 1 (RACK1) in actin cytoskeleton dynamics and *Shigella* infection. We used time-lapse imaging to demonstrate that RACK1 facilitates *Shigella*-induced actin cytoskeleton remodeling at multiple levels during infection of epithelial cells. Silencing RACK1 expression impaired *Shigella*-induced rapid polymerizing structures, reducing host cell invasion, bacterial motility, and cell-to-cell spreading. In uninfected cells, RACK1 silencing reduced jasplakinolide-mediated filamentous actin aggregate formation and negatively affected actin turnover in fast polymerizing structures, such as membrane ruffles. Our findings provide a role of RACK1 in actin cytoskeleton dynamics and *Shigella* infection.**

INTRODUCTION

The bacterial pathogen *Shigella flexneri* (hereafter referred to as *Shigella)* extensively manipulates host functions to invade the colonic epithelium.[1] *Shigella* employs a type 3 secretion system (T3SS) to inject bacterial effectors into the host cytosol, exploiting host cell pathways of actin nucleation, polymerization, and depolymerization.[2] The initial steps in bacterial entry involve the effectors IpaB and IpaC, which induce massive actin polymerization at the primary entry site (focus), resulting in large membrane ruffles that engulf bacteria.[3] This process requires IpaC-mediated activation of the host kinase Sarcoma (Src) kinase as well as Rac family small GTPase 1 (Rac1) and cell division cycle 42 (Cdc42). Active Rac1 and Cdc42 subsequently recruit the actin related protein 2/3 (Arp2/3) complex.[3–6] The Arp2/3 complex binds to pre-formed actin filaments and triggers actin polymerization, forming filament branches.[7] The binding of IpaC and subsequent activation of Src has been further linked to cortactin phosphorylation.[8] Active cortactin then recruits the Arp2/3 complex, inducing actin polymerization.[9] Actin depolymerization at the entry focus, driven by the effector IpaA, is also critical for bacterial invasion.[10,11]

After host cell invasion, *Shigella* briefly resides within the endocytic vacuole. During this time, the bacterium induces IcsB-driven actin polymerization around the *Shigella*-containing vacuole (SCV), forming a cocoon-like structure. The actin cocoon rapidly depolymerizes, allowing bacterial escape from the vacuole.[12] In the cytosol, *Shigella* utilizes its adhesin IcsA to induce actin polymerization at one pole of the bacterium, forming an actin "tail". IcsA mediates recruitment and activation of the neuronal Wiskott-Aldrich syndrome protein (N-WASP), followed by recruitment of the Arp2/3 complex to activate actin polymerization.[13–15] *Shigella*'s actin tail propels the bacterium within the host cytosol, allowing actin-mediated motility, eventually leading to engagement and deformation of the host cell membrane into *Shigella*-containing protrusions.[16] These protrusions are then endocytosed by neighboring host cells, leading to secondary infections.[17,18] Within the secondarily infected cell, *Shigella* escapes a double-membrane vacuole formed by the membranes from the primary infected cell and the secondary infected cell.[19,20] Following these events, *Shigella* continues infection cycles by replicating, nucleating actin tails, and forming protrusions to infect more cells.[20]

The puzzle of *Shigella*-host interactions is not complete, and it is likely to involve other host factors modulating the host cytoskeleton during the successive invasion steps. For example, the host receptor for activated C kinase 1 (RACK1), a tryptophan-aspartate repeat (WD-repeat) seven-bladed β-propeller protein, interacts with various protein partners, including cytoskeleton proteins.[21–23] RACK1 mediates focal

[1]Department of Microbiology and Immunology, Dalhousie University, Halifax, NS B3H 4R2, Canada
[2]Unité Dynamique des interactions hôtes-pathogènes, Institut Pasteur and CNRS UMR3691, Université de Paris-Cité, 75724 Paris, France
[3]Department of Applied Oral Sciences, Dalhousie University, Halifax, NS B3H 4R2, Canada
[4]Present address: Division of Molecular and Cellular Biology, Eunice Kennedy Shriver National Institute of Child Health and Human Development, National Institutes of Health, Bethesda, MD 20892, USA
[5]Lead contact
*Correspondence: zhenyu.cheng@dal.ca
https://doi.org/10.1016/j.isci.2023.108216

adhesion formation by promoting the interaction of Src and the focal adhesion kinase (FAK).[24] Focal adhesions are active sites for actin polymerization controlled by Rac1, Ras homologous (Rho), and Cdc42, forming attachment structures that link internal actin bundles called stress fibers to the extracellular matrix.[25] The host cell cytoskeleton machinery and its related proteins are prone to be targeted by *Shigella* virulence factors, making RACK1 an interesting host factor to study in the context of *Shigella*-triggered cytoskeleton reorganization and infection.

Furthermore, RACK1 has been shown to interact with bacterial virulence factors. RACK1 acts as an immune sensor of *Mycobacterium tuberculosis* effector EST12, triggering cell death via pyroptosis, whereas RACK1's interaction with *Yersinia pseudotuberculosis* effector YopK protects bacteria from phagocytosis. RACK1 is required for innate immune pathway activation in *Caenorhabditis elegans* infected with *Shigella*[26,27]; however, this model organism is grown at temperatures that do not sustain *Shigella*'s T3SS. Despite these reports, the roles of RACK1 during bacterial and specifically its role in *Shigella* infection remain poorly understood.

Here we demonstrate that RACK1 promotes *Shigella* infection and facilitates actin polymerization in infected cells. We used time-lapse microscopy techniques and automated image data analysis to study the dynamics of *Shigella* infection in RACK1-depleted epithelial cells. RACK1 silencing impacted distinct steps of the process of bacterial internalization and infection. Silencing RACK1 expression reduced actin polymerization at *Shigella*'s entry site, impairing invasion. We observed a defect in *Shigella*'s actin tail polymerization and actin-mediated motility in RACK1-silenced cells, leading to a cell-to-cell spreading impairment. We also examined the general role of RACK1 in actin cytoskeleton dynamics in uninfected cells. When inducing actin filament stabilization with jasplakinolide, RACK1-silenced cells had less filamentous actin (F-actin) aggregate formation, suggesting a delay in actin polymerization. Finally, analysis of actin turnover measured by fluorescence recovery after photobleaching (FRAP) showed that RACK1 promotes actin turnover in membrane ruffles but not in stress fibers formed in uninfected cells. Overall, our work reveals a previously unknown function of RACK1 in actin polymerization by aiding the formation of fast-polymerizing actin structures, such as *Shigella*-induced entry foci and actin tails during bacterial infection, as well as membrane ruffles in uninfected cells.

RESULTS

RACK1 facilitates *Shigella* growth in HeLa cells

To determine whether RACK1 plays a role in *Shigella* pathogenesis, we took a genetic approach to silence RACK1 expression in HeLa cells using short hairpin RNAs (shRNAs) delivered by a lentiviral vector (pLKO). The shRNAs, designed to target different sections of the RACK1 mRNA (KD-92, KD-94, and KD-95), successfully reduced the relative expression of RACK1 compared with the control cells transduced with a non-specific shRNA (NS, Figure 1A). Furthermore, we confirmed that RACK1 silencing does not interfere with tubulin or actin expression levels (Figure 1A) and does not impact cell size (Figure S1). The stable RACK1-knockdown (KD) HeLa cell lines generated were then used to evaluate the role of RACK1 in *Shigella* infection. Growth curves determined by gentamicin protection assay showed fewer colony-forming units (CFU) of *Shigella* recovered from RACK1-KD than from NS cells and significantly lower growth rate (Figure 1B). While three knockdown cell lines were used in this work, the cell line KD-92 was chosen for most experiments, such as the genetic complementation discussed below, due to its stable knockdown of RACK1 expression. *Shigella* growth was restored by incorporating a recombinant copy of *RACK1* gene into the genome of the KD-92 cells using lentiviruses (pLJM1:RACK1). Gene expression, driven by the cytomegalovirus (CMV) promoter, was sufficient to re-establish RACK1 expression levels to control (NS) levels in the KD-92 cell line (Figure 1C). Recovering RACK1 expression rescued the growth defect of *Shigella* in KD-92 cells (Figure 1D).

Interestingly, we observed increased *Shigella* growth in NS cells transduced with pLJM1:RACK1 lentivirus compared with NS alone (Figure 1D). This finding prompted the investigation of RACK1 overexpression effects on *Shigella* infection. Due to difficulties in maintaining stable overexpression of RACK1, we instead performed transient overexpression in HeLa cells transfected with the high-expression plasmid pEGFP harboring N- and C-terminus GFP-tagged RACK1. Forty-eight hours after transfection, these cells were infected with *Shigella*, and growth was evaluated by gentamicin assay. Western blot analysis confirmed the expression of the fusion proteins (GFP-RACK1, RACK1-GFP, Figure 1E). Consistent with the results observed in NS cells stably expressing recombinant RACK1 (Figure 1D), transient overexpression of GFP-tagged RACK1 promoted *Shigella* growth, resulting in significantly higher bacterial load than transfection reagent control (Figure 1F). Taken together, the RACK1 silencing, complementation, and overexpression experiments suggest that RACK1 plays an important role for efficient *Shigella* growth within HeLa cells.

RACK1 recruitment to *Shigella*'s entry focus is required for efficient HeLa cell invasion

Then, we set out to investigate how RACK1 affected *Shigella*'s intracellular growth cycle. To invade epithelial cells, *Shigella* forms an entry focus by triggering profuse fast actin polymerization and host membrane ruffles, which subsequently engulf the bacterium.[6,28] This process is mediated by multiple bacterial and host cell factors.[6,29] Given that RACK1 is involved in focal adhesion regulation, we evaluated the role of RACK1 during *Shigella*-induced cytoskeleton modifications at the entry focus. Time-lapse imaging was performed to determine if RACK1 was recruited to entry foci. For this, HeLa cells stably expressing RACK1-GFP and F-tractin-mCherry (F-tractin is a peptide derived from the rat neuronal inositol 1,4,5-triphosphate 3-kinase A that binds actin filaments[30]) were imaged every 60 s for 1.5 h after infection with *Shigella*. Figure 2A shows selected images from a time-lapse of a HeLa cell infected by *Shigella* (Video S1). Although the bacterium was not fluorescently labeled, actin foci formed during *Shigella* invasion could be readily spotted (Figure 2A, yellow rectangle). The fluorescence intensity (FI) change over time was measured in a specific region of interest (ROI) centered around an entry focus, confirming that RACK1 and actin were recruited simultaneously to the entry focus (yellow rectangle in Figures 2A and 2B).

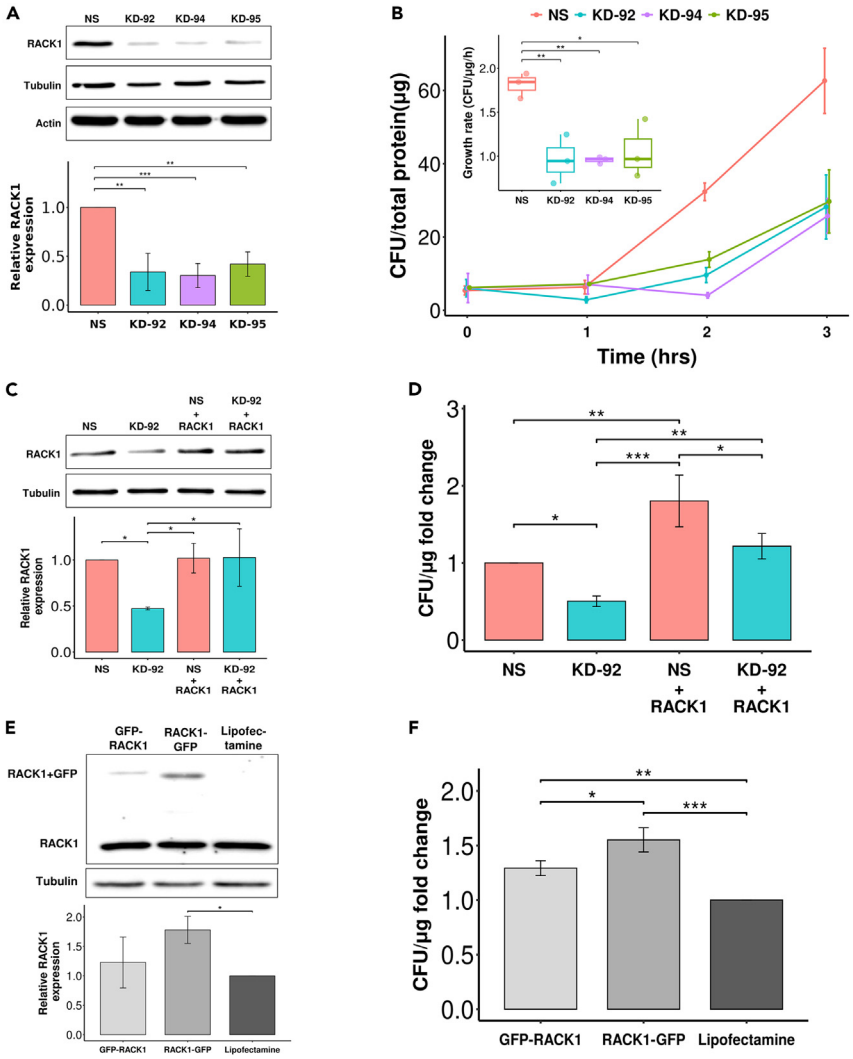

Figure 1. RACK1 promotes *Shigella* growth in HeLa cells

(A) Top: immunoblot confirming RACK1 silencing in HeLa cells. Anti-tubulin and anti-actin antibodies were used as loading controls. Bottom: fold change in RACK1 expression was calculated relative to tubulin. One-way ANOVA followed by TukeyHSD; ***p < 0.001, ****p < 0.0001. See also Figure S1.

(B) Representative growth curves of *Shigella* in RACK1-silenced HeLa cells. Colony-forming units (CFU) were normalized by total protein/well to account for cells lost during washes. Error bars are mean ± standard deviation (SD) from one representative experiment in triplicate. Inset: *Shigella* growth rate (CFU/µg/h). One-way ANOVA and TukeyHSD; *p < 0.05, **p < 0.01.

(C) Top: immunoblot showing RACK1 expression restoration in RACK1-KD-92 cells transduced with lentiviruses carrying pLJM1:RACK1 plasmid. Bottom: fold change in RACK1 expression relative to tubulin. Error bars are mean ± SD from 3 separate blots. Two-way ANOVA and TukeyHSD; *p < 0.05.

(D) Expression of pLJM1:RACK1 in RACK1-KD-92 cells restores *Shigella* growth in HeLa cells at 2 h postinfection. Error bars are mean ± SD from 3 independent experiments. Two-way ANOVA and TukeyHSD; *p < 0.05, **p < 0.01, ***p < 0.001.

(E) Top: immunoblot confirming expression of GFP-tagged RACK1 in HeLa cells. Anti-Tubulin was the loading control. Bottom: fold change in RACK1 expression. Error bars are mean ± SD from 3 separate blots. One-way ANOVA and TukeyHSD; *p < 0.05.

(F) *Shigella* growth is enhanced in HeLa cells transiently expressing GFP-tagged RACK1. CFU/mL were measured at 2 h postinfection and normalized by total protein/well to account for cells lost during washes. Error bars are mean ± SD from three separate experiments. One-way ANOVA and TukeyHSD; *p < 0.05, **p < 0.01, ***p < 0.001.

After cell invasion, *Shigella* damages the SCV and escapes into the cytosol, where it replicates. This process triggers the recruitment of the host lectin galectin-3 (Gal-3) that binds to damaged membranes (Figure 2C).[31] We evaluated if RACK1 was involved in vacuolar escape by measuring the time between entry and recruitment of Gal-3 to the SCV. Immunofluorescence analysis showed RACK1 is not recruited to Gal-3-positive SCVs (Figure S2A). Damaged SCVs become Gal-3 positive (Gal-3$^+$) between 5 and 10 min after *Shigella* internalization into HeLa cells, followed by release into the host cytosol (Figure S2B).[12,28] RACK1 silencing did not alter the average time of bacterial escape

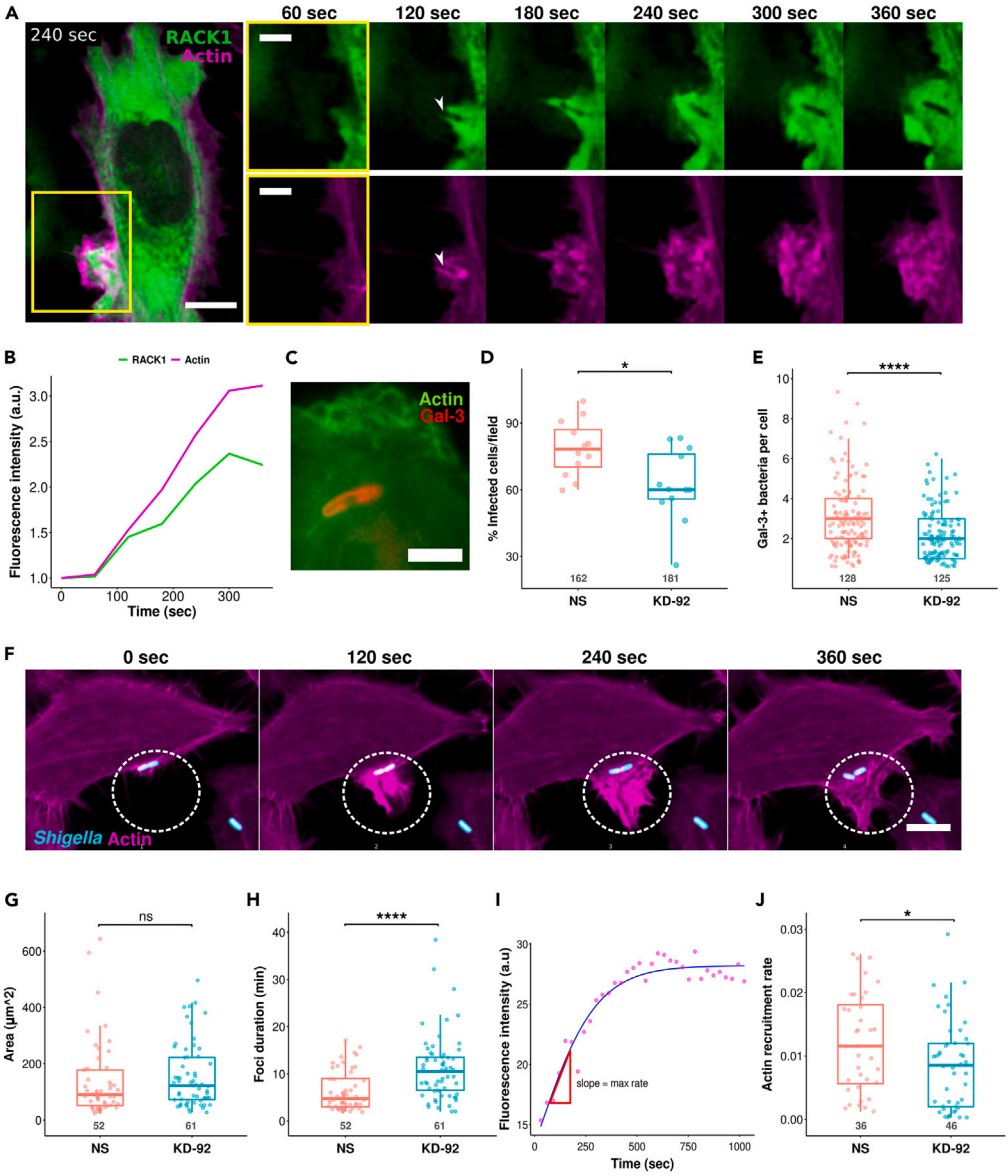

Figure 2. RACK1 silencing alters *Shigella*'s entry focus formation dynamics and reduces bacterial invasion of HeLa cells

(A) RACK1 is recruited to the entry focus. Selected confocal images from a time-lapse showing RACK1-GFP (top) and mCherry-F-tractin (bottom) recruitment to *Shigella*'s entry site (yellow rectangle). Scale bars, 5 µm (right) and 10 µm (left). White arrowheads show non-fluorescent *Shigella*. See also Video S1.

(B) Fluorescence intensity (FI) change over time in the rectangular area highlighted in A shows simultaneous recruitment of RACK1 (green) and actin (magenta) to *Shigella*'s entry site. FI was normalized by dividing each time point value by the cell's average FI per μm^2 before *Shigella* entry.

(C) HeLa cell transfected with pmOrange-Galectin3 (red) and pEGFP-Actin (green). The micrograph shows galectin-3 (Gal-3) recruitment to the SCV upon vacuole rupture. Scale bar, 5 µm. See also Figure S2.

(D) RACK1 silencing reduces the percentage (%) of *Shigella*-infected HeLa cells. Dots are the % of infected cells found in one field of view out of 12 per condition. Total number of cells analyzed in three separate experiments are shown under each plot. Unpaired t test *$p < 0.05$. See also Figure S3.

(E) RACK1 silencing reduces the number of entry events as shown by less Gal-3-positive SCV per infected HeLa cell found in KD-92 compared with NS. The number of infected cells analyzed, pooled from 3 separate experiments, are shown under the plots. Wilcoxon rank-sum test; ****$p < 0.0001$.

(F) Confocal images from a time-lapse showing profuse actin recruitment (magenta) to *Shigella*'s entry site. The bacteria are shown in cyan. The images are maximum projections of the original z stack. White dotted-line ovals mark a region of interest (ROI) enclosing the boundaries of the entry focus at its maximum area (240-s time point). Scale bar, 10 µm.

(G) RACK1 silencing does not affect the maximum area of *Shigella*'s entry foci. Maximum area was determined as shown in F. Numbers under plots are the foci analyzed in one representative experiment out of three. Wilcoxon rank-sum test; ns = not significant.

(H) RACK1 silencing increases foci duration. Numbers under plots are the foci analyzed in one representative experiment out of three. Wilcoxon rank-sum test; ****$p < 0.0001$.

Figure 2. *Continued*

(I and J) RACK1 silencing reduces the rate of actin recruitment to the entry focus. (I) Pink dots are actual FI values. The maximum rate (max. rate) of actin recruitment was calculated as the slope of the fitted curve (blue line) obtained with a logistic model. a.u. = arbitrary units. (J) Actin recruitment rate to entry foci calculated as described in I. Numbers under the boxplots are the foci analyzed in one representative experiment out of three. Wilcoxon rank-sum test; *$p < 0.05$.

into the cytosol, which was around 8.5 min (Figures S2B and S2C). These results suggest that the growth inhibition phenotype observed in RACK1-silenced cells is likely not caused by vacuolar escape impairment.

Given that RACK1 was recruited to the entry site, we reasoned that silencing RACK1 expression could negatively impact bacterial invasion. To test this, we captured 1.5 h of time-lapse videos post-inoculation with bacteria and quantified the percentage of successfully infected cells. Some bacteria enter the host cell but fail to rupture the vacuole: therefore, entry-focus identification alone is not an appropriate marker of cell invasion. We showed that RACK1 does not interfere with SCV escape (Figure S2). Therefore, assuming all viable invading bacteria should escape toward the cytosol, Gal-3 recruitment to the SCV was an ideal marker for invasion as it shows infection progression (Figure 2C). We classified cells as being infected if they had at least one Gal-3^+ SCV during the 1.5 h time-lapse video captured (Figure 2C). The RACK1 KD-92 condition had ~17% (62.1% $\pm$ 16.4%) fewer infected cells than the control condition (78.6% $\pm$ 12.5%, Figure 2D). We also quantified the number of Gal-3^+ SCVs per cell. Control NS cells had, on average, 3 $\pm$ 2 Gal-3^+ SCV per cell, whereas KD-92 cells had 2 $\pm$ 1 Gal-3^+ SCV per cell (Figure 2E), confirming a reduction of *Shigella* invasiveness upon RACK1 silencing. *Shigella* invasion of epithelial cells can be dependent or independent of actin tails. The primary invasion event does not involve actin tail polymerization, whereas subsequent invasion of neighboring cells (secondary invasion event) is actin-tail-dependent. We used Δ*icsA-Shigella*, a mutant that is unable to induce actin tail polymerization, to evaluate primary entry. RACK1 silencing significantly reduced the number of cells containing Δ*icsA-Shigella*, indicating that RACK1 is involved in primary infection events (Figure S3).

Shigella induces rapid and profuse actin polymerization at the entry site, resulting in filamentous (F)-actin accumulation in F-actin foci structures. The F-actin focus increases on size over time until *Shigella* is completely internalized (Figure 2F), followed by focus resolution and plasma membrane basal state recovery. We hypothesized that RACK1 silencing leads to alterations in actin dynamics required for entry focus formation, reducing cell invasion. To test this, we evaluated the dynamics of *Shigella*-induced entry foci using time-lapse imaging. HeLa cells expressing F-tractin-GFP were infected with dsRED-*Shigella* and imaged every 2 min for 1.5 h. The maximum expansion of each entry focus was encircled to create an ROI (Figure 2F, dotted-line oval) from which the area was calculated. No significant differences were found in the maximum area of the foci formed in KD-92 (154 $\pm$ 113 μm^2) and NS cells (137 $\pm$ 133 μm^2, Figure 2G). However, when measuring the duration while the entry foci remained visible, we found that foci formed in KD-92 cells lasted significantly longer (11.1 $\pm$ 7.02 min) than in NS cells (6.29 $\pm$ 4.19 min, Figure 2H).

To further understand how RACK1 modulates foci formation, we quantified the rate of actin recruitment at the entry site. The FI of the focus could be interpreted as the amount of F-actin polymerized around *Shigella* during entry. We used a logistic model to estimate the maximum rate of actin recruitment (F-actin polymerization) based on the FI changes observed on each infection focus over time. Figure 2I shows an example of an entry focus FI curve (dots) and the best-fitted curve (blue line), from which the maximum rate of F-actin recruitment was calculated. The logistic regression analysis revealed a modest but significant reduction in the actin recruitment rate in KD-92 cells (0.0085 $\pm$ 0.007 s^{-1}) compared with NS cells (0.0121 $\pm$ 0.008 s^{-1}, Figure 2J), suggesting that RACK1 is required for efficient actin polymerization around bacteria during foci formation. A slow actin recruitment rate in the KD-92 cells likely extends entry foci duration (Figures 2H and 2J) until enough actin polymerization has occurred, increasing the focus area to maximum size before *Shigella* can be internalized.

RACK1 is required for actin tail polymerization and actin-mediated motility without localizing to the actin tail

Because RACK1 was required for actin recruitment to the *Shigella* invasion site, we sought to investigate whether RACK1 is also required for actin tail formation. We first evaluated RACK1 recruitment to *Shigella*'s actin tail. After a thorough analysis of multiple lines of experiments, including time-lapse microscopy of cells co-expressing RACK1-GFP and F-tractin-mCherry (Video S2) and confocal imaging of fixed samples, no colocalization between the actin tail and RACK1 was found (Figure 3A). This shows that RACK1 is likely not a structural component of *Shigella*'s actin tail. However, given that actin polymerization at the entry site was RACK1-dependent, we further evaluated whether RACK1 silencing impacts actin tail polymerization in both HeLa cells and the colonic epithelial cell line CaCo-2. The same three shRNAs (KD-92, KD-94, and KD-95) used in HeLa cells successfully reduced the relative expression of RACK1 compared with the control cells transduced with the non-specific shRNA in CaCo-2 cells (Figure S4). NS and KD-92 HeLa and CaCo-2 cells were infected with dsRED-*Shigella* for 3 h to allow actin tail formation in a large portion of infected cells. Then, cells were fixed and stained with phalloidin-Alexa647 to detect F-actin. As expected, most *Shigella* within NS cells were associated with an actin tail. In contrast, most *Shigella* appeared untailed in KD-92 cells (Figure 3B). Quantification of tailed and untailed bacteria confirmed this observation. On average, in HeLa cells, 42.4% $\pm$ 15.1% of bacteria were associated with an actin tail in NS, whereas this percentage was reduced to 24.8% $\pm$ 12.5% in KD-92 cells (Figure 3C, left). Similarly, the percentage of tailed bacteria was significantly reduced in CaCo-2 cells upon silencing of RACK1 (62.2% $\pm$ 5.4% in NS and 37.6% $\pm$ 6.9% in KD-92) (Figure 3C, right). These findings suggest that RACK1 is required for actin tail polymerization.

Given that the actin tails formed in CaCo-2 cells are less prominent than those formed in HeLa, we characterized the length and FI of the tails formed in HeLa cells only. For this analysis, the perimeters of the *Shigella* tails were manually outlined to generate ROIs from which Feret's diameter and FI were measured. The Feret's diameter was defined as the longest distance between two points along the tail's boundary

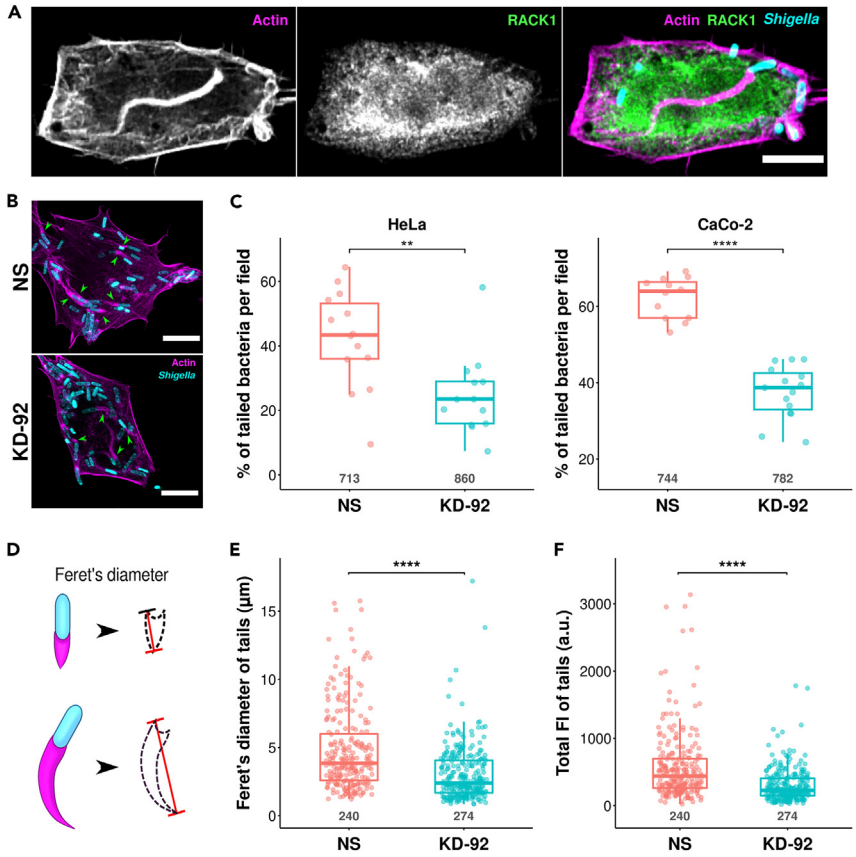

Figure 3. RACK1 does not localize to *Shigella*'s actin tail but it is required for efficient actin tail polymerization

(A) Confocal images of a HeLa cell infected with *Shigella* (cyan) showing RACK1 (green) does not co-localize to the actin tail (magenta). Scale bar, 8 µm. See also Video S2.

(B and C) RACK1 silencing reduces the number of tailed *Shigella*. (B) Representative confocal images of NS and KD-92 HeLa cells infected with dsRED-*Shigella*. Green arrowheads indicate bacteria (cyan) associated with actin tails (magenta). Scale bar, 10 µm. (C) Percentage of tailed *Shigella* per field of view in HeLa (left) and CaCo-2 cells (right). Numbers under the boxplots are total bacteria counted, pooled from four separate experiments. Unpaired t test; **p < 0.01, ***p < 0.001. See also Figure S4.

(D and E) RACK1 silencing in HeLa cells impairs actin tail elongation. (D) Schematic of Feret's diameter (red segment) calculation. Diagrams of *Shigella* with short (top) and long (bottom) actin tails are shown. (E) Feret's diameter of actin tails formed in NS and KD-92 HeLa cells. Numbers under plots show the actin tails analyzed, pooled from three separate experiments. Wilcoxon rank-sum test; ****p < 0.0001.

(F) RACK1 silencing in HeLa cells reduces actin tail fluorescence. Total fluorescence intensity (FI) of actin tails formed in NS and KD-92 HeLa cells was calculated as the product of tail's area and average FI. Numbers under plots are actin tails analyzed, pooled from three separate experiments. Wilcoxon rank-sum test; ****p < 0.0001.

(Figure 3D) and was used to estimate tail length. Actin tails formed in NS cells had a significantly higher Feret's diameter (4.91 ± 3.2 µm) than tails in KD-92 cells (3 ± 1.9 µm, Figure 3E). Furthermore, we calculated the total FI of the actin tails and found the tails formed in KD-92 cells had lower total FI than those formed in NS cells (Figure 3F). The higher total FI values of tails formed in control cells indicate either brighter tails or the same FI on a larger area, supporting the Feret's diameter data. These findings indicate RACK1 promotes actin tail polymerization and elongation.

We measured the actin-based motility of *Shigella* within infected cells to determine whether the decrease in actin tail length and total FI observed in RACK1-KD cells affected bacterial motility. NS and KD-92 HeLa cells expressing F-tractin-GFP were infected with *Shigella* and imaged every 60 s for 2 h. Bacteria were manually tracked from the moment they formed an actin tail until they stopped moving for more than 5 consecutive frames (Figure 4A). Spatial locations were grouped into bacterial trajectories. Visual inspection of the trajectories displayed in an x,y coordinate plot (starting point 0,0) readily showed distinct patterns. *Shigella* trajectories were more linear, appeared more dispersed from the center of the plot, and exhibited more rapid movements (cyan) in NS cells than in KD-92 cells (Figure 4B). Indeed, the speed of *Shigella* in RACK1-KD cells (0.03 ± 0.021 µm/s) was 33.3% less compared with the NS cells (0.045 ± 0.021 µm/s, Figure 4C).

In addition to speed, bacterial trajectories can also be characterized based on their tortuosity.[32] The sinuosity index describes a trajectory's tortuosity, integrating changes of direction and step lengths (distance between 2 measured bacterial positions).[32] More frequent

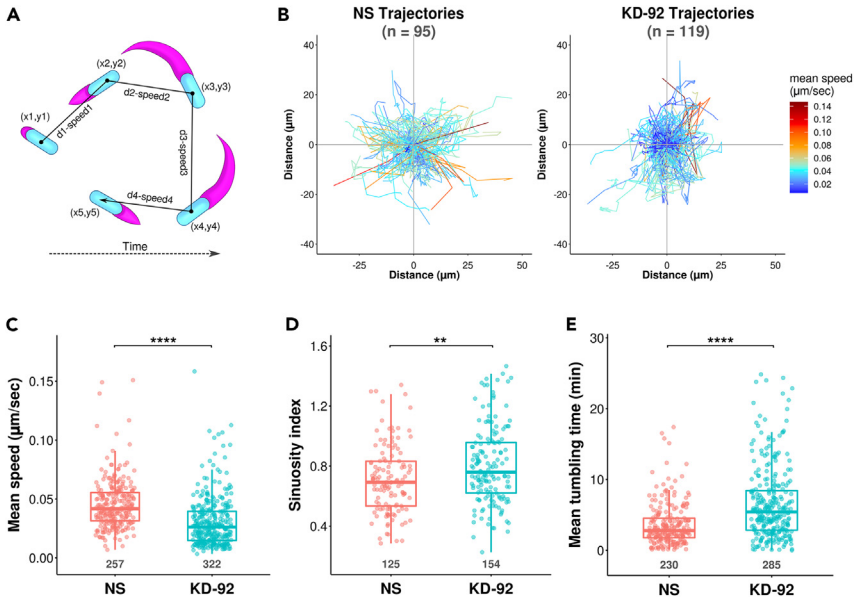

Figure 4. RACK1 silencing impairs *Shigella*'s actin-mediated motility

(A) Schematics of *Shigella* (cyan) trajectory displaying multiple direction changes and actin-tail (magenta) lengths.

(B) *Shigella* trajectories from one representative experiment. Colors represent trajectories' mean speed (µm/s).

(C) RACK1 silencing reduces the speed of *Shigella* movements. Numbers under plots are trajectories pooled from three separate experiments. Wilcoxon rank-sum test; ****$p < 0.0001$.

(D) *Shigella* trajectories show higher sinuosity in RACK1-KD cells. Trajectories with lengths between 30 and 80 µm pooled from three independent experiments were analyzed (number below boxplots). Unpaired t test; **$p < 0.01$.

(E) RACK1 silencing increases the time *Shigella* expends tumbling. Trajectories with one or more tumbling events were selected for this analysis. Plots show trajectories pooled from three independent experiments (number of evaluated trajectories under boxplots). Wilcoxon rank-sum test; ****$p < 0.0001$.

reorientation events and a broader distribution of reorientation angles lead to less direct (more tortuous/sinuous) trajectories. A low sinuosity index indicates a more direct trajectory. Given that longer trajectories are inevitably more tortuous than very short trajectories, we selected trajectories with lengths between 30 and 80 µm to calculate sinuosity. Interestingly, *Shigella* trajectories were significantly more tortuous in KD-92 cells (0.81 ± 0.26) than in control cells (0.71 ± 0.23, Figure 4D), suggesting RACK1 promotes trajectory straightness.

We reasoned that the higher trajectory tortuosity observed in the KD-92 cells could be caused by bacterial tumbling. Tumbles are stopping events characteristic of bacterial motility that result in an erratic change of the trajectory's direction.[33] Tumbling events in *Shigella*'s trajectories were identified by setting a minimum speed threshold of 0.02 µm/s. Typically, *Shigella*'s trajectories were interrupted by one or more tumble event (speed <0.02 µm/s). The tumbles can be consecutive or intermittent. We quantified the average time bacteria spent in static state (tumbling) and found that *Shigella*'s trajectories were interrupted by significantly more tumble events in KD-92 cells than in control cells (Figure 4E). *Shigella* spent on average 3.6 ± 3 min tumbling in NS cells, whereas tumbling time was doubled in KD-92 cells (6.6 ± 5 min, Figure 4E). While recording the trajectories, we observed that bacterial motility stops when *Shigella* loses or reduces the length of its tail. To resume movement, *Shigella* must induce actin tail polymerization again. Thus, extended tumbling events found in RACK1-KD cells are consistent with an actin-tail polymerization defect, delaying motility (Figures 3B and 3C).

RACK1 silencing inhibits *Shigella* cell-to-cell spreading

Shigella's cell-to-cell spreading relies on efficient actin tail polymerization as the tail accelerates the bacterium to reach the host cell's periphery, pushing the membrane out to form *Shigella*-containing membrane protrusions subsequently endocytosed by neighboring cells.[18,34] Therefore, we reasoned that the actin tail polymerization and intracellular motility impairment observed in RACK1-KD cells could affect *Shigella* cell-to-cell spreading. To evaluate this, we implemented a modified plaque assay that allows time-lapse imaging of *Shigella* spreading. Briefly, confluent cell monolayers stably expressing GFP were infected with a low-density dsRED-*Shigella* culture (OD_{600} diluted to ~0.0005 in imaging medium). Methocel, a non-toxic transparent polymer, was used to overlay the cells restricting *Shigella*'s extracellular diffusion. As *Shigella* spreads through the cell monolayer, it forms areas of infection called plaques. The size of these plaques correlates with the efficiency of bacterial cell-to-cell spreading.[35] Because *Shigella* cells were fluorescent, our plaque assay did not require fixation or staining steps for visualization, and we used automatic segmentation for plaque area quantification. Conveniently, the 96-well format of our plaque assay allowed simultaneous analysis of control (NS) and three stable RACK-KD cell lines (KD-92, KD-94, and KD-95). Significant reduction in plaque area was observed in all three RACK1-KD HeLa cells (Figures 5A and 5B). We also evaluated *Shigella* cell-to-cell

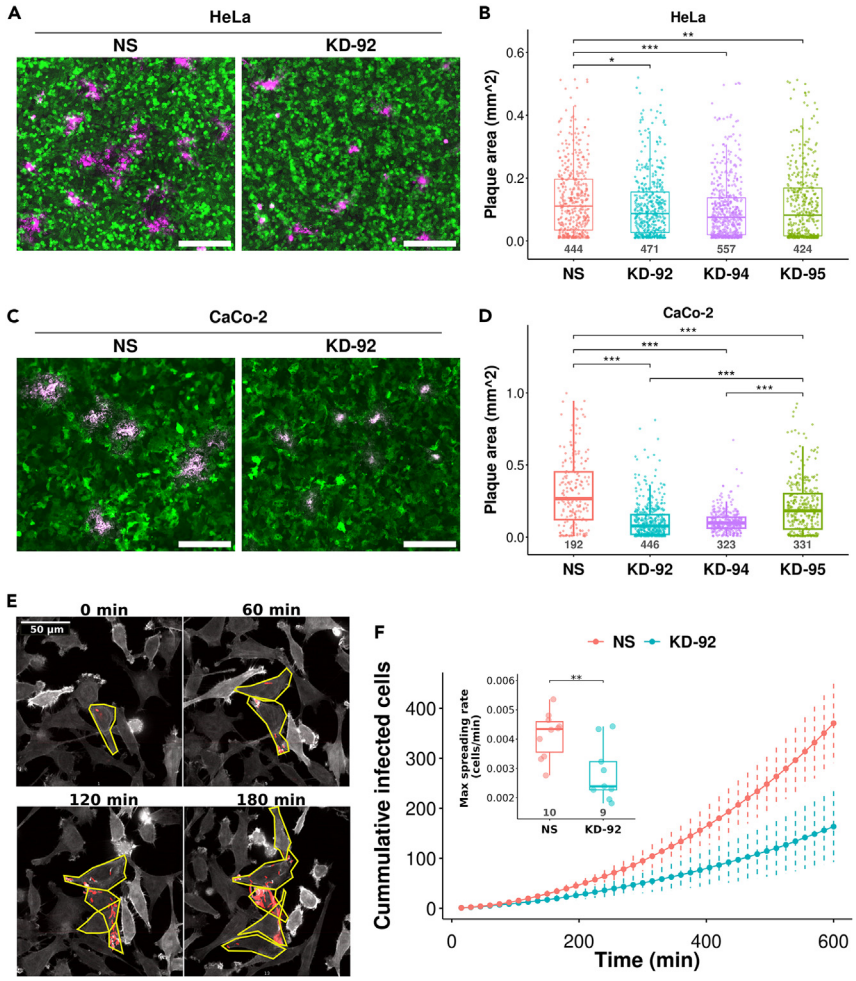

Figure 5. RACK1 silencing reduces *Shigella* cell-to-cell spreading in HeLa and CaCo-2 cells

(A) Representative images showing dsRED-*Shigella* plaques (magenta) formed in control (NS) and RACK1-KD (KD-92) HeLa cells (F-tractin-GFP, green). Scale bar, 300 µm.

(B) RACK1-KD leads to plaque area reduction in HeLa cells. Plots show representative data from one out of three separate experiments. Numbers under the boxplots are the numbers of plaques analyzed. Kruskal-Wallis followed by Dunn's test; *p < 0.05, **p < 0.01, ***p < 0.001.

(C) Representative images of dsRED-*Shigella* plaques (magenta) formed in control (NS) and RACK1-KD (KD-92) CaCo-2 cells (GFP, green). Scale bar, 300 µm.

(D) RACK1-KD leads to plaque area reduction in CaCo-2 cells. Plots are from one out of three separate experiments. Numbers under the boxplots are the numbers of plaques analyzed. Kruskal-Wallis and Dunn's test; ***p < 0.001.

(E and F) *Shigella* cell-to-cell spreading is reduced in RACK1-silenced HeLa cells. (E) Representative time-lapse images showing dsRED-*Shigella* (red) cell-to-cell spreading. Actin is shown in gray. Yellow outlines highlight the infected cells. (F) Cumulative number of infected cells over time. Cell-to-cell spreading curves are shown as mean ± SD from three experiments pooled, where 19 (NS = 10, KD-92 = 9) infection videos were analyzed. Inset: maximum spreading rate (infected cells/min) was calculated. Unpaired t test; **p < 0.01.

spreading in CaCo-2 cells. Like in HeLa cells, *Shigella* formed significantly smaller plaques in RACK1-KD cells than in the NS control (Figures 5C and 5D).

To further examine the impact of RACK1 silencing on *Shigella* spreading, we captured high magnification (63X) time-lapse images of infected cells overlaid with Methocel. We then manually recorded infection progression (Figure 5E). Analysis of the cumulative number of infected cells recorded over 10 h of infection showed a significant reduction of *Shigella*'s dissemination rate in KD-92 cells compared with NS cells (Figure 5F). Altogether, these results indicate that RACK1 contributes to effective *Shigella* cell-to-cell dissemination in epithelial cells.

RACK1 promotes actin polymerization in uninfected cells

Our findings in *Shigella*-infected cells suggest that RACK1 is likely a regulator of actin cytoskeleton dynamics. We then evaluated whether RACK1 plays a role in actin polymerization independently of *Shigella* infection. Actin filaments are maintained in a dynamic equilibrium of polymerization and depolymerization, also known as actin filament turnover. The filaments elongate as ATP-bound G-actin monomers are

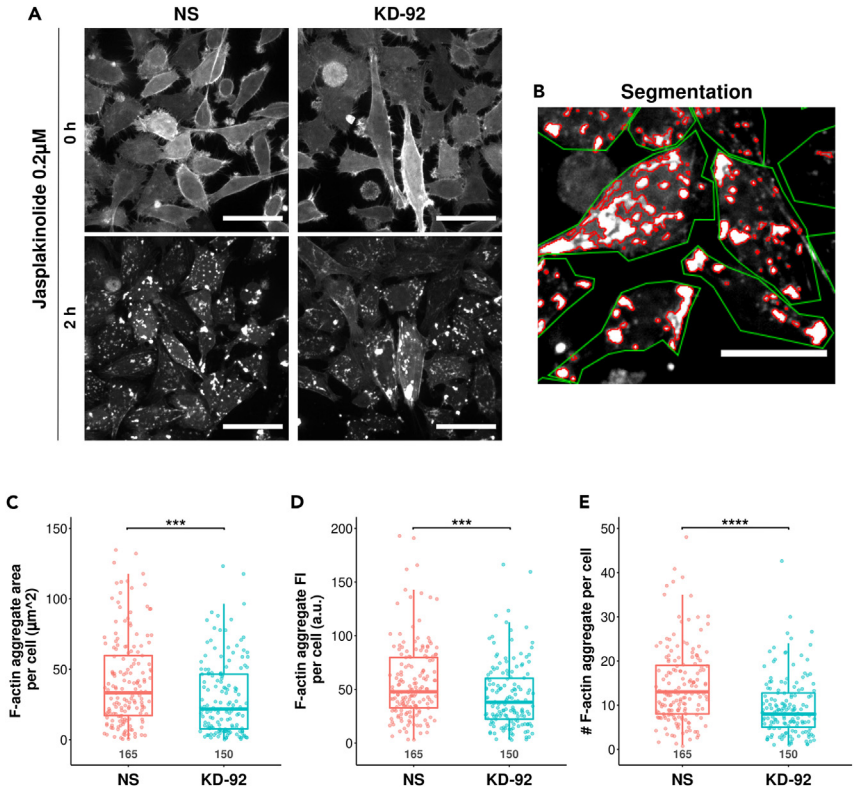

Figure 6. Filamentous-actin (F-actin) aggregate formation is reduced in uninfected RACK1-KD cells treated with jasplakinolide

(A) Representative maximum projection images of control (NS) and RACK1-KD (KD-92) HeLa cells at 0 h and 2 h after 0.2 μM of jasplakinolide (Jasp) treatment. Actin is shown in gray. Scale bar, 50 μm.

(B) Example of F-actin (gray) aggregate automatic segmentation (red outlines). Cells' outlines (green) were manually drawn. Scale bar, 30 μm.

(C) The area of F-actin aggregates formed per cell is reduced in RACK1-silenced cells.

(D) The total fluorescence intensity (FI) of F-actin aggregates formed per cell is reduced in RACK1-silenced cells. Aggregate FI was normalized to the average FI of cells before the addition of Jasp.

(E) The number (#) of F-actin aggregates per cell is reduced in RACK1-silenced cells.

Numbers under the boxplots in C–D indicate the number of cells analyzed, pooled from 2 independent experiments. Wilcoxon rank-sum test; ***$p < 0.001$, ****$p < 0.0001$.

added to the filament's fast-growing barbed end, whereas ADP-bound G-actin is dissociated from the slow-growing pointed end.[36] We used the actin-binding compound jasplakinolide (Jasp) to evaluate the role of RACK1 in actin polymerization. Jasp stabilizes F-actin by inhibiting filament depolymerization, thereby inducing the formation of F-actin amorphous aggregates.[37] Treatment with 0.2 μM of Jasp for 2 h caused the formation of multiple F-actin aggregates throughout the cytoplasm in NS and KD-92 HeLa cells (Figure 6A). These aggregates were quantified using automatic segmentation (Figure 6B). We reasoned that if RACK1 promotes actin polymerization, RACK1-KD cells should be less susceptible to the effect of Jasp-mediated aggregate formation. Indeed, the F-actin aggregates formed in KD-92 cells were smaller and dimmer than those in NS cells (Figures 6C and 6D). Also, the number of aggregates formed was reduced in KD-92 cells. On average, 14 ± 9 actin aggregates were found per NS cells, whereas 10 ± 7 aggregates were found per KD-92 cells, suggesting that RACK1 facilitates filament polymerization (Figure 6E).

To further understand the role of RACK1 in actin polymerization, we evaluated the effect of RACK1 silencing on actin turnover in basal conditions (i.e., uninfected cells). Fluorescence recovery after photobleaching (FRAP) has been widely used to analyze actin polymerization dynamics.[38] FRAP was assessed in two characteristic actin-rich cellular structures, membrane ruffles and stress fibers. HeLa cells transfected with EGFP-actin were photo-bleached in a rectangular region of interest (ROI), and the fluorescence recovery was followed by time-lapse imaging (Figure 7A, red rectangles). EGFP-actin fluorescence was fast to recover in membrane ruffles (~6 s), indicating fast actin turnover in these structures, whereas stress fibers had a slower actin turnover rate (~180 s, Figure 7A). We then evaluated actin turnover in RACK1-silenced cells. The fitted recovery curves obtained from membrane ruffles revealed slower actin turnover in KD-92 than in NS cells (Figure 7B, left). A significant difference was confirmed by calculating the half-time of fluorescence recovery (t1/2), which was lower in NS cells (11.3 ± 4.6 s) than in KD-92 cells (30.2 ± 8.2 s, Figure 7B, right), indicating RACK1 promotes actin turnover in membrane ruffles. On the other hand, no significant difference was found in stress fiber actin turnover between NS (t1/2 = 16.1 ± 9.3) and KD-92 (t1/2 = 20 ± 11.3) cells (Figure 7C). These results show that RACK1 is required for efficient actin turnover in fast-polymerizing structures such as membrane ruffles but not in stress

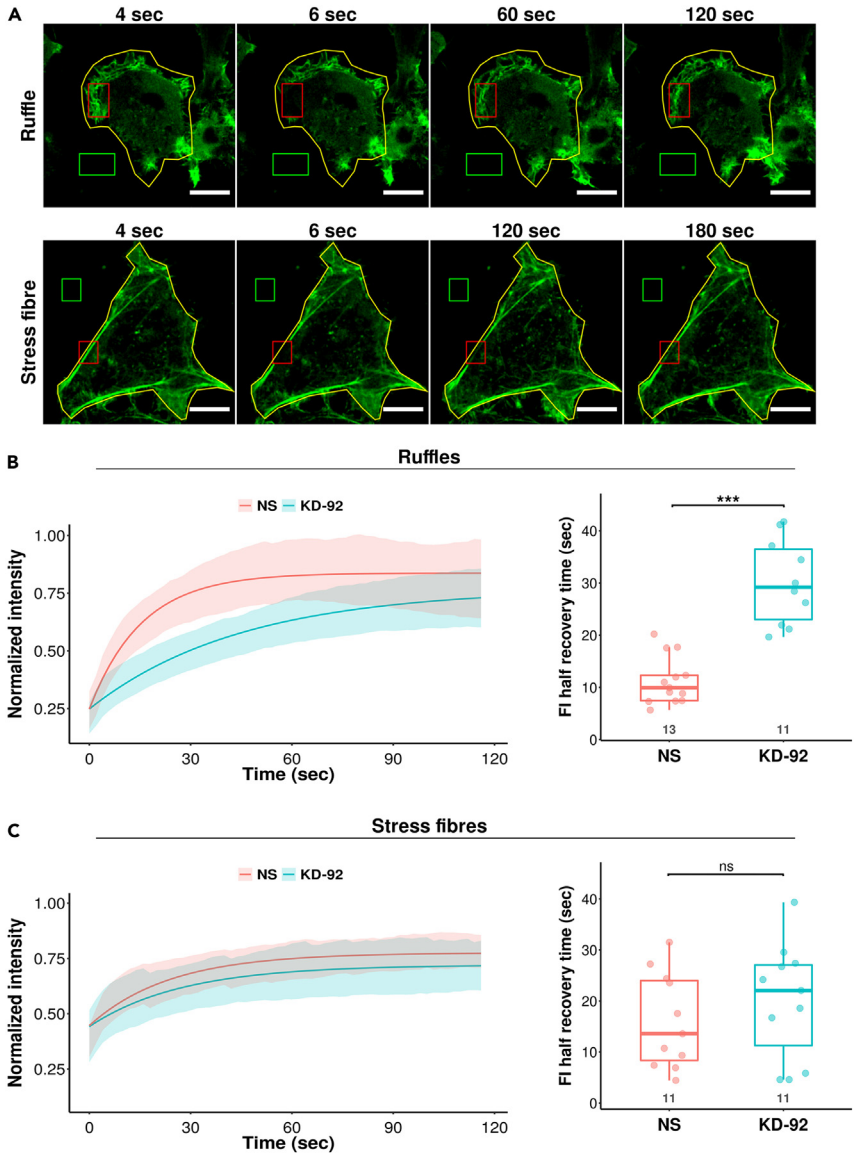

Figure 7. RACK1 silencing affects actin turnover in membrane ruffles but not in stress fibers

(A) Selected confocal images from a time-lapse showing fluorescence recovery after photobleaching (FRAP) of EGFP-actin in ruffles (top) and stress fibers (bottom). Red rectangles show the bleached area. The whole cell is outlined in yellow, and background (cell-free area) areas are shown in green rectangles. Scale bar, 10 μm.

(B and C) In the line plots, solid lines represent best-fit curves, and ribbons show the mean ± SD of the samples analyzed. Boxplots show half-time fluorescence intensity (FI) recovery. Numbers under the boxplots represent the number of cells analyzed per condition. Unpaired t test; ns = not significant; ****p < 0.0001. (B) RACK1 silencing increases EGFP-actin fluorescence recovery time in ruffles naturally formed in uninfected HeLa cells. (C) RACK1 silencing does not impact EGFP-Actin fluorescence recovery in the stress fibers of uninfected HeLa cells.

fiber formation. Membrane ruffles occur in cellular areas undergoing rapid actin cytoskeleton reorganization and very much resemble *Shigella*-induced entry foci.[3] Actin tails are also fast-polymerizing structures allowing *Shigella* to move at high speeds (0.045 ± 0.021 μm/s in control cells, Figure 4C). Overall, our data show that RACK1 is required for physiological and *Shigella*-induced fast-polymerizing actin structures.

DISCUSSION

In this study, we investigated the role of the host scaffold protein RACK1 in *Shigella flexneri* infection of epithelial cells. Our findings also lead us to explore the role of RACK1 in cytoskeleton organization in uninfected conditions. We showed via gentamycin assay that silencing RACK1

expression significantly reduces *Shigella* growth in HeLa cells, whereas overexpression of RACK1 leads to more *Shigella* growth (Figure 1). Time-lapse microscopy analysis showed that RACK1 localization to the entry focus is crucial for efficient actin recruitment around *Shigella*, thus facilitating invasion (Figure 2). We also showed that actin tail polymerization, tail elongation, actin-based motility, and cell-to-cell spreading are negatively impacted by RACK1 silencing (Figures 3, 4, and 5). Our data demonstrate that RACK1 is involved in multiple steps of *Shigella* infection that share a requirement for actin cytoskeleton machinery and may collectively contribute to the positive correlation between RACK1 expression and the overall intracellular amount of *Shigella*. Our analysis of actin dynamics in physiological conditions (uninfected cells) revealed that RACK1 silencing reduces F-actin aggregate formation in response to jasplakinolide treatment and impairs actin turnover in fast-polymerizing structures such as membrane ruffles (Figures 6 and 7). Together, these results suggest a crucial role of RACK1 in actin cytoskeleton modulation, promoting the formation of fast-polymerizing structures during *Shigella* infection and in physiological conditions.

Shigella invasiveness is mediated by the T3SS proteins IpaC and IpaB, which form a pore into the host cell membrane, allowing bacterial effectors to be translocated inside the host cell. IpaC recruits the host kinase Src to the entry foci, leading to rapid actin polymerization and ruffle formation.[6] Similar to what was observed in RACK1-silenced cells, the expression of kinase-inactive Src in HeLa cells inhibits foci formation and *Shigella* uptake.[39] The Abelson tyrosine kinase (Abl) has also been linked to *Shigella*'s uptake. Abl phosphorylates Crk, which binds to cortactin, triggering Arp2/3-mediated actin polymerization and subsequent bacterial internalization.[40] Because RACK1 plays a key role in stabilizing the inactive or active form of various kinases including Abl and Src,[22,41,42] it is likely that RACK1 facilitates actin polymerization responsible for forming host membrane ruffles that engulf *Shigella*. In support of this hypothesis, we found that RACK1 silencing significantly reduces the rate of actin polymerization during *Shigella*-induced entry foci formation and impairs actin turnover in membrane ruffles (Figures 2J and 7B). The crosstalk between RACK1, Abl, and Src signaling during *Shigella*-induced actin polymerization at the entry site remains to be evaluated by further studies.

After *Shigella* uptake into the host cell, the bacterium briefly remains in the SCV. A thick F-actin-rich cage, coined as a cocoon, was recently described to form around the SCV.[12] Actin cocoon formation has been linked to vacuolar rupture by *Shigella*, and as we did not observe an impact of RACK1 knockdown on the SCV rupture timing, we decided not to follow-up on a potential link between the actin cocoon and RACK1. The next step after *Shigella*'s vacuolar escape is actin-mediated motility, which eventually leads to infection of neighboring cells. We found RACK1 silencing was associated with a decrease in the percentage of bacteria forming actin tails, with shortening of tails and speed reduction of motile bacteria (Figures 3 and 4). Although RACK1 seems to participate in actin tail formation, it was not recruited to the tail (Figure 3A), suggesting its role is indirect. *In vitro* reconstitution of actin polymerization using purified proteins determined that actin, N-WASP, Arp2/3, cofilin, and capping protein are the minimal required factors for *Shigella*'s actin tail polymerization.[43] However, other host proteins have been reported to enable more efficient actin tail formation and intracellular motility, such as, the transducer of Cdc42-dependent actin assembly (Toca-1), Bruton's tyrosine kinase (Btk), and Abl.[44–46] These proteins, like RACK1, have not been shown to be detectable at the actin tails, although it cannot be completely ruled out that these proteins could be part of actin tails under certain experimental conditions.

The Abl kinase plays a crucial part not only in *Shigella* entry of host cells but also in promoting the polymerization and elongation of actin tails via N-WASP phosphorylation.[45] Bacterial speed decreases by 48% in cells without Abl,[45] similar to the 33.3% reduction that we observed in RACK1-KD cells. We postulate that RACK1 could promote actin tail polymerization and actin-mediated motility by stabilizing Abl in its active conformation, leading to N-WASP phosphorylation. Efficient formation of actin tails is pivotal for bacterial spreading to neighbouring cells. Our study shows that RACK1 depletion in HeLa and CaCo-2 cells impairs cell-to-cell spreading (Figure 5). This is an expected phenotype because *Shigella*-containing membrane protrusions leading to dissemination seem to result solely from the force exerted by the actin tail deforming the host plasma membrane.[20]

In the host cell cytoplasm, when *Shigella* loses the actin tail and starts replicating, the bacteria can be recognized by septins that trap them inside septin cages, blocking actin tail polymerization.[47] Septins are host cytoskeletal proteins that assemble into filaments, bundles, and rings implicated in cell division.[48] In RACK1-silenced cells, *Shigella* may struggle to recover its actin tail due to septin cage entrapment, spending a long time tumbling (Figure 4E). Mostowy et al. found that more tailed bacteria were present in septin-depleted cells but no alteration in speed was observed, suggesting septins restrict tail elongation but not bacterial movement.[49] The authors reported an average speed of 0.3 μm/s, which is 6 times faster than our observations (0.045 μm/s). This difference is likely due to the methodology used. We measured the average speed of trajectories recorded from images taken every 1 min for 2 h, whereas Mostowy et al. measured trajectories for 15 min (images taken every 10 s). In this manner, the authors likely missed tumbling intervals commonly observed in *Shigella* trajectories (Figure 4E). We showed that RACK1 depletion slowed down actin polymerization. This could provide sufficient time for septins to detect *Shigella* and initiate cage formation. Still, the role of septin-mediated restriction of *Shigella*'s intracellular growth and motility requires further study.

In addition to *Shigella*-induced actin polymerization, when RACK is silenced in uninfected cells, we found less F-actin aggregate formation upon Jasplakinolide treatment and impaired actin turnover in membrane ruffles (Figures 6 and 7). Other reports have linked RACK1 to actin cytoskeleton dynamics. For example, preventing the interaction of RACK1 with Src disrupts the actin cytoskeleton in embryonic mouse fibroblast NIH3T3 cells.[50] Also, RACK1 promotes cytoskeletal reorganization in osteoclasts. In these cells, overexpression of a mutant RACK1 that does not bind to Src reduces the formation of actin rings.[51] Similarly, RACK1 silencing in mast cells induces cell rounding and fragmentation of cortical F-actin.[52]

The cellular machinery required for fast-polymerizing actin structures, such as those found in the entry focus, actin tail, and membrane ruffles, are governed by Abl and Src kinases[6,39,45,53,54] through Cdc42/Rac1-mediated activation of N-WASP.[55] N-WASP subsequently

activates the Arp2/3 complex to promote actin polymerization. Because RACK1 was shown to regulate Abl and Src activation,[42,50,56] it is possible that RACK1 activity promotes actin turnover in highly dynamic structures rather than stable ones such as stress fibers (Figure 7C). This finding was intriguing as RACK1 overexpression has been reported to increase the number of stress fibers in CHO cells.[57] However, actin polymerization in stress fibers is regulated by the small GTPase RhoA and its effectors Rho-associated protein kinase (ROCK) and Dia1.[58,59] There are conflicting reports about the link between RACK1 and RhoA. In breast cancer cells, RACK1 was shown to promote migration through interaction with RhoA and activation of the RhoA/Rho kinase pathway,[60] whereas RACK1 silencing in Jurkat cells does not affect RhoA activation. These findings suggest that RACK1-mediated regulation of RhoA is cell-type-specific. Our data show that, at least in HeLa cells, RACK1 does not regulate stress fiber formation.

Our results demonstrate that RACK1 is essential for *Shigella* infection by facilitating actin recruitment to the site of infection, actin tail polymerization, actin-based motility, and cell-to-cell spreading in human epithelial cells. Collectively, our work supports a pro-virulence role of RACK1 for *Shigella* through facilitating actin polymerization and a physiological role in actin cytoskeleton dynamics. Future studies will help decipher the mechanism by which RACK1 regulates actin cytoskeleton dynamics in uninfected conditions and during *Shigella* infection, a process most likely mediated by RACK1-kinase interactions.

Limitations of the study

In this study, we found that *Shigella* exploits the function of RACK1 to promote bacterial entry, actin tail formation, and cell-to-cell spreading. However, the mechanism by which RACK1 regulates actin cytoskeleton dynamics in *Shigella*-infected cells was not elucidated. We proposed a mechanism involving the RACK1-interacting partners Abl and Src kinases. However, whether these kinases are the link between *Shigella*-mediated actin manipulation and RACK1 remains to be validated in future studies. We also revealed an interesting role of RACK in regulating actin turnover in rapidly polymerizing actin structures. To gain more insights, further analysis of actin turnover, recruitment of actin polymerization proteins to cell ruffles, and subsequent disassembly of actin structures will need to be assessed.

STAR★METHODS

Detailed methods are provided in the online version of this paper and include the following:

- KEY RESOURCES TABLE
- RESOURCE AVAILABILITY
  - Lead contact
  - Materials availability
  - Data and code availability
- EXPERIMENTAL MODEL AND STUDY PARTICIPANT DETAILS
  - Cell lines culture
  - *Shigella* strains culture
- METHOD DETAILS
  - Recombinant DNA and lentiviral transduction
  - RACK1 expression assessment by western blotting
  - Gentamycin protection assay to measure intracellular *Shigella* growth
  - Time-lapse confocal microscopy of *Shigella* invasion
  - Primary infection evaluation
  - Immunofluorescence of infected epithelial cells for actin tail evaluation
  - Time-lapse confocal microscopy of *Shigella* actin-mediated motility
  - Evaluation of *Shigella* cell-to-cell spreading via plaque assay
  - Evaluation of actin polymerization in uninfected cells
- QUANTIFICATION AND STATISTICAL ANALYSIS

SUPPLEMENTAL INFORMATION

Supplemental information can be found online at https://doi.org/10.1016/j.isci.2023.108216.

ACKNOWLEDGMENTS

The work was supported by the Natural Sciences and Engineering Research Council of Canada (NSERC) of Canada Discovery Grants (grant number: RGPIN/04912-2016) and Canadian Institutes of Health Research Project Grant (grant number: PJT165970) to Z.C. J.E., thanks to the European Research Council (ERC-CoG EndoSubvert), the Agene National pour la Recherche (Grants: PureMagRupture, RabReprogram), and the LabEx programs IBEID and Milieu Interieure. Y.Y.C. has been supported by a grant from the Fondation pour la Recherche Médicale (FRM); K.V. is a recipient of a Chilean government doctorate scholarship (Scholarship number: 72160538) and Mitacs Globalink Research Award. We thank Stephen Whitefield and Brianne Lindsay at the Cellular & Molecular Digital Imaging (CMDI) core facility of Dalhousie's Faculty of Medicine for their assistance in microscopy experiments and technical support. K.V. also acknowledges the help with microscopy training received

by Dr. Laura Barrio Cano and Dr. Sonja Kühn at the Unité Dynamique des interactions hôtes-pathogènes, Institut Pasteur, Paris, France. We thank Dr. Andrew Stadnyk at Dalhousie University for providing the CaCo-2 cell line.

AUTHOR CONTRIBUTIONS

Conceptualization: K.N.V., J.R.R., and Z.C.; Methodology: K.N.V., E.F, Y.C., R.R., and Y.S.; Software: K.N.V.; Formal Analysis: K.V.; Investigation: K.V.; Resources: Z.C., J.R.R, J.E, and B.M.L.; Writing—Original Draft: K.V.; Writing—Review & Editing Preparation: K.V., Z.C., J.R.R, Y.C., and J.E.; Visualization: K.V.; Supervision: Z.C., J.R.R, Y.C., and J.E.; Funding Acquisition: Z.C. and J.E.

DECLARATION OF INTERESTS

The authors declare no competing interests.

INCLUSION AND DIVERSITY

We support inclusive, diverse, and equitable conduct of research.

Received: April 28, 2023
Revised: August 19, 2023
Accepted: October 11, 2023
Published: October 14, 2023

REFERENCES

1. Bhavsar, A.P., Guttman, J.A., and Finlay, B.B. (2007). Manipulation of host-cell pathways by bacterial pathogens. Nature *449*, 827–834. https://doi.org/10.1038/nature06247.
2. Valencia-Gallardo, C.M., Carayol, N., and Tran Van Nhieu, G. (2015). Cytoskeletal mechanics during Shigella invasion and dissemination in epithelial cells. Cell Microbiol. *17*, 174–182. https://doi.org/10.1111/cmi.12400.
3. Tran Van Nhieu, G., Caron, E., Hall, A., and Sansonetti, P.J. (1999). IpaC induces actin polymerization and filopodia formation during Shigella entry into epithelial cells. EMBO J. *18*, 3249–3262. https://doi.org/10.1093/emboj/18.12.3249.
4. Mounier, J., Laurent, V., Hall, A., Fort, P., Carlier, M.F., Sansonetti, P.J., and Egile, C. (1999). Rho family GTPases control entry of Shigella flexneri into epithelial cells but not intracellular motility. J. Cell Sci. *112*, 2069–2080. https://doi.org/10.1242/jcs.112.13.2069.
5. Terry, C.M., Picking, W.L., Birket, S.E., Flentie, K., Hoffman, B.M., Barker, J.R., and Picking, W.D. (2008). The C-terminus of IpaC is required for effector activities related to Shigella invasion of host cells. Microb. Pathog. *45*, 282–289. https://doi.org/10.1016/j.micpath.2008.06.003.
6. Mounier, J., Popoff, M.R., Enninga, J., Frame, M.C., Sansonetti, P.J., and Van Nhieu, G.T. (2009). The IpaC Carboxyterminal Effector Domain Mediates Src-Dependent Actin Polymerization during Shigella Invasion of Epithelial Cells. PLoS Pathog. *5*, e1000271. https://doi.org/10.1371/journal.ppat.1000271.
7. Goley, E.D., and Welch, M.D. (2006). The ARP2/3 complex: an actin nucleator comes of age. Nat. Rev. Mol. Cell Biol. *7*, 713–726. https://doi.org/10.1038/nrm2026.
8. Dehio, C., Prévost, M.C., and Sansonetti, P.J. (1995). Invasion of epithelial cells by Shigella flexneri induces tyrosine phosphorylation of cortactin by a pp60c-src-mediated signalling pathway. EMBO J. *14*, 2471–2482. https://doi.org/10.1002/j.1460-2075.1995.tb07244.x.
9. Bougnères, L., Girardin, S.E., Weed, S.A., Karginov, A.V., Olivo-Marin, J.-C., Parsons, J.T., Sansonetti, P.J., and Van Nhieu, G.T. (2004). Cortactin and Crk cooperate to trigger actin polymerization during Shigella invasion of epithelial cells. J. Cell Biol. *166*, 225–235. https://doi.org/10.1083/jcb.200402073.
10. Tran Van Nhieu, G., Ben-Ze'ev, A., and Sansonetti, P.J. (1997). Modulation of bacterial entry into epithelial cells by association between vinculin and the Shigella IpaA invasin. EMBO J. *16*, 2717–2729. https://doi.org/10.1093/emboj/16.10.2717.
11. Bourdet-Sicard, R., Rüdiger, M., Jockusch, B.M., Gounon, P., Sansonetti, P.J., and Nhieu, G.T. (1999). Binding of the Shigella protein IpaA to vinculin induces F-actin depolymerization. EMBO J. *18*, 5853–5862. https://doi.org/10.1093/emboj/18.21.5853.
12. Kühn, S., Bergqvist, J., Gil, M., Valenzuela, C., Barrio, L., Lebreton, S., Zurzolo, C., and Enninga, J. (2020). Actin Assembly around the Shigella-Containing Vacuole Promotes Successful Infection. Cell Rep. *31*, 107638. https://doi.org/10.1016/j.celrep.2020.107638.
13. Goldberg, M.B., and Theriot, J.A. (1995). Shigella flexneri surface protein IcsA is sufficient to direct actin-based motility. Proc. Natl. Acad. Sci. USA *92*, 6572–6576. https://doi.org/10.1073/pnas.92.14.6572.
14. Goldberg, M.B., Bârzu, O., Parsot, C., and Sansonetti, P.J. (1993). Unipolar localization and ATPase activity of IcsA, a Shigella flexneri protein involved in intracellular movement. J. Bacteriol. *175*, 2189–2196. https://doi.org/10.1128/jb.175.8.2189-2196.1993.
15. Suzuki, T., Mimuro, H., Suetsugu, S., Miki, H., Takenawa, T., and Sasakawa, C. (2002). Neural Wiskott-Aldrich syndrome protein (N-WASP) is the specific ligand for Shigella VirG among the WASP family and determines the host cell type allowing actin-based spreading. Cell Microbiol. *4*, 223–233. https://doi.org/10.1046/j.1462-5822.2002.00185.x.
16. Bernardini, M.L., Mounier, J., d'Hauteville, H., Coquis-Rondon, M., and Sansonetti, P.J. (1989). Identification of icsA, a plasmid locus of Shigella flexneri that governs bacterial intra- and intercellular spread through interaction with F-actin. Proc. Natl. Acad. Sci. USA *86*, 3867–3871. https://doi.org/10.1073/pnas.86.10.3867.
17. Kadurugamuwa, J.L., Rohde, M., Wehland, J., and Timmis, K.N. (1991). Intercellular spread of Shigella flexneri through a monolayer mediated by membranous protrusions and associated with reorganization of the cytoskeletal protein vinculin. Infect. Immun. *59*, 3463–3471. https://doi.org/10.1128/iai.59.10.3463-3471.1991.
18. Fukumatsu, M., Ogawa, M., Arakawa, S., Suzuki, M., Nakayama, K., Shimizu, S., Kim, M., Mimuro, H., and Sasakawa, C. (2012). Shigella Targets Epithelial Tricellular Junctions and Uses a Noncanonical Clathrin-Dependent Endocytic Pathway to Spread Between Cells. Cell Host Microbe *11*, 325–336. https://doi.org/10.1016/j.chom.2012.03.001.
19. Kuehl, C.J., Dragoi, A.-M., and Agaisse, H. (2014). The Shigella flexneri type 3 secretion system is required for tyrosine kinase-dependent protrusion resolution, and vacuole escape during bacterial dissemination. PLoS One *9*, e112738. https://doi.org/10.1371/journal.pone.0112738.
20. Monack, D.M., and Theriot, J.A. (2001). Actin-based motility is sufficient for bacterial membrane protrusion formation and host cell uptake. Cell Microbiol. *3*, 633–647. https://doi.org/10.1046/j.1462-5822.2001.00143.x.
21. Carrillo, D.R., Chandrasekaran, R., Nilsson, M., Cornvik, T., Liew, C.W., Tan, S.M., and Lescar, J. (2012). Structure of human Rack1 protein at a resolution of 2.45 Å. Acta Crystallogr. Sect. F *68*, 867–872. https://doi.org/10.1107/S1744309112027480.
22. Adams, D.R., Ron, D., and Kiely, P.A. (2011). RACK1, A multifaceted scaffolding protein: Structure and function. Cell Commun. Signal. *9*, 22. https://doi.org/10.1186/1478-811X-9-22.
23. Ron, D., Adams, D.R., Baillie, G.S., Long, A., O'Connor, R., and Kiely, P.A. (2013). RACK(1)

to the future – a historical perspective. Cell Commun. Signal. *11*, 53. https://doi.org/10.1186/1478-811X-11-53.

24. Serrels, B., Sandilands, E., Serrels, A., Baillie, G., Houslay, M.D., Brunton, V.G., Canel, M., Machesky, L.M., Anderson, K.I., and Frame, M.C. (2010). A complex between FAK, RACK1, and PDE4D5 controls spreading initiation and cancer cell polarity. Curr. Biol. *20*, 1086–1092. https://doi.org/10.1016/j.cub.2010.04.042.
25. Nobes, C.D., and Hall, A. (1995). Rho, rac, and cdc42 GTPases regulate the assembly of multimolecular focal complexes associated with actin stress fibers, lamellipodia, and filopodia. Cell *81*, 53–62. https://doi.org/10.1016/0092-8674(95)90370-4.
26. Marudhupandiyan, S., Prithika, U., Balasubramaniam, B., and Balamurugan, K. (2017). RACK-1, a multifaceted regulator is required for C. elegans innate immunity against S. flexneri M9OT infection. Dev. Comp. Immunol. *74*, 227–236. https://doi.org/10.1016/j.dci.2017.05.008.
27. Kesika, P., Karutha Pandian, S., and Balamurugan, K. (2011). Analysis of Shigella flexneri-mediated infections in model organism Caenorhabditis elegans. Scand. J. Infect. Dis. *43*, 286–295. https://doi.org/10.3109/00365548.2010.548400.
28. Ehsani, S., Santos, J.C., Rodrigues, C.D., Henriques, R., Audry, L., Zimmer, C., Sansonetti, P., Tran Van Nhieu, G., and Enninga, J. (2012). Hierarchies of host factor dynamics at the entry site of Shigella flexneri during host cell invasion. Infect. Immun. *80*, 2548–2557. https://doi.org/10.1128/IAI.06391-11.
29. Lee, J.H., Park, H., and Park, Y.H. (2014). Molecular Mechanisms of Host Cytoskeletal Rearrangements by Shigella Invasins. Int. J. Mol. Sci. *15*, 18253–18266. https://doi.org/10.3390/ijms151018253.
30. Schell, M.J., Erneux, C., and Irvine, R.F. (2001). Inositol 1,4,5-trisphosphate 3-kinase A associates with F-actin and dendritic spines via its N terminus. J. Biol. Chem. *276*, 37537–37546. https://doi.org/10.1074/jbc.M104101200.
31. Paz, I., Sachse, M., Dupont, N., Mounier, J., Cederfur, C., Enninga, J., Leffler, H., Poirier, F., Prevost, M.-C., Lafont, F., and Sansonetti, P. (2010). Galectin-3, a marker for vacuole lysis by invasive pathogens. Cell Microbiol. *12*, 530–544. https://doi.org/10.1111/j.1462-5822.2009.01415.x.
32. Benhamou, S. (2004). How to reliably estimate the tortuosity of an animal's path: straightness, sinuosity, or fractal dimension? J. Theor. Biol. *229*, 209–220. https://doi.org/10.1016/j.jtbi.2004.03.016.
33. Taute, K.M., Gude, S., Tans, S.J., and Shimizu, T.S. (2015). High-throughput 3D tracking of bacteria on a standard phase contrast microscope. Nat. Commun. *6*, 8776. https://doi.org/10.1038/ncomms9776.
34. Agaisse, H. (2016). Molecular and Cellular Mechanisms of Shigella flexneri Dissemination. Front. Cell. Infect. Microbiol. *6*, *29*. https://doi.org/10.3389/fcimb.2016.00029.
35. Sharma, A., and Puhar, A. (2019). Plaque Assay to Determine Invasion and Intercellular Dissemination of Shigella flexneri in TC7 Human Intestinal Epithelial Cells. Bio. Protoc. *9*, e3293. https://doi.org/10.21769/BioProtoc.3293.
36. Amann, K.J., and Pollard, T.D. (2000). Cellular regulation of actin network assembly. Curr. Biol. *10*, R728–R730. https://doi.org/10.1016/s0960-9822(00)00751-x.
37. Lázaro-Diéguez, F., Aguado, C., Mato, E., Sánchez-Ruíz, Y., Esteban, I., Alberch, J., Knecht, E., and Egea, G. (2008). Dynamics of an F-actin aggresome generated by the actin-stabilizing toxin jasplakinolide. J. Cell Sci. *121*, 1415–1425. https://doi.org/10.1242/jcs.017665.
38. Hardy, L.R. (2012). Fluorescence recovery after photobleaching (FRAP) with a focus on F-actin. Curr. Protoc. Neurosci. *Chapter 2*. Unit 2.17. https://doi.org/10.1002/0471142301.ns0217s61.
39. Duménil, G., Olivo, J.C., Pellegrini, S., Fellous, M., Sansonetti, P.J., and Nhieu, G.T. (1998). Interferon α Inhibits a Src-mediated Pathway Necessary for Shigella-induced Cytoskeletal Rearrangements in Epithelial Cells. J. Cell Biol. *143*, 1003–1012. https://doi.org/10.1083/jcb.143.4.1003.
40. Burton, E.A., Plattner, R., and Pendergast, A.M. (2003). Abl tyrosine kinases are required for infection by Shigella flexneri. EMBO J. *22*, 5471–5479. https://doi.org/10.1093/emboj/cdg512.
41. Chang, B.Y., Chiang, M., and Cartwright, C.A. (2001). The interaction of Src and RACK1 is enhanced by activation of protein kinase C and tyrosine phosphorylation of RACK1. J. Biol. Chem. *276*, 20346–20356. https://doi.org/10.1074/jbc.M101375200.
42. Kiely, P.A., Baillie, G.S., Barrett, R., Buckley, D.A., Adams, D.R., Houslay, M.D., and O'Connor, R. (2009). Phosphorylation of RACK1 on tyrosine 52 by c-Abl is required for insulin-like growth factor I-mediated regulation of focal adhesion kinase. J. Biol. Chem. *284*, 20263–20274. https://doi.org/10.1074/jbc.M109.017640.
43. Loisel, T.P., Boujemaa, R., Pantaloni, D., and Carlier, M.F. (1999). Reconstitution of actin-based motility of Listeria and Shigella using pure proteins. Nature *401*, 613–616. https://doi.org/10.1038/44183.
44. Leung, Y., Ally, S., and Goldberg, M.B. (2008). Bacterial Actin Assembly Requires Toca-1 to Relieve N-WASP Autoinhibition. Cell Host Microbe *3*, 39–47. https://doi.org/10.1016/j.chom.2007.10.011.
45. Burton, E.A., Oliver, T.N., and Pendergast, A.M. (2005). Abl kinases regulate actin comet tail elongation via an N-WASP-dependent pathway. Mol. Cell Biol. *25*, 8834–8843. https://doi.org/10.1128/MCB.25.20.8834-8843.2005.
46. Dragoi, A.-M., Talman, A.M., and Agaisse, H. (2013). Bruton's Tyrosine Kinase Regulates Shigella flexneri Dissemination in HT-29 Intestinal Cells. Infect. Immun. *81*, 598–607. https://doi.org/10.1128/IAI.00853-12.
47. Krokowski, S., Lobato-Márquez, D., Chastanet, A., Pereira, P.M., Angelis, D., Galea, D., Larrouy-Maumus, G., Henriques, R., Spiliotis, E.T., Carballido-López, R., and Mostowy, S. (2018). Septins Recognize and Entrap Dividing Bacterial Cells for Delivery to Lysosomes. Cell Host Microbe *24*, 866–874.e4. https://doi.org/10.1016/j.chom.2018.11.005.
48. Mostowy, S., and Cossart, P. (2012). Septins: the fourth component of the cytoskeleton. Nat. Rev. Mol. Cell Biol. *13*, 183–194. https://doi.org/10.1038/nrm3284.
49. Mostowy, S., Bonazzi, M., Hamon, M.A., Tham, T.N., Mallet, A., Lelek, M., Gouin, E., Demangel, C., Brosch, R., Zimmer, C., et al. (2010). Entrapment of intracytosolic bacteria by septin cage-like structures. Cell Host Microbe *8*, 433–444. https://doi.org/10.1016/j.chom.2010.10.009.
50. Miller, L.D., Lee, K.C., Mochly-Rosen, D., and Cartwright, C.A. (2004). RACK1 regulates Src-mediated Sam68 and p190RhoGAP signaling. Oncogene *23*, 5682–5686. https://doi.org/10.1038/sj.onc.1207735.
51. Park, J.H., Jeong, E., Lin, J., Ko, R., Kim, J.H., Yi, S., Choi, Y., Kang, I.-C., Lee, D., and Lee, S.Y. (2019). RACK1 interaction with c-Src is essential for osteoclast function. Exp. Mol. Med. *51*, 1–9. https://doi.org/10.1038/s12276-019-0285-4.
52. Filho, E.G.F., da Silva, E.Z.M., Ong, H.L., Swaim, W.D., Ambudkar, I.S., Oliver, C., and Jamur, M.C. (2021). RACK1 plays a critical role in mast cell secretion and Ca2+ mobilization by modulating F-actin dynamics. J. Cell Sci. *134*, jcs252585. https://doi.org/10.1242/jcs.252585.
53. Srinivasan, D., and Plattner, R. (2006). Activation of Abl tyrosine kinases promotes invasion of aggressive breast cancer cells. Cancer Res. *66*, 5648–5655. https://doi.org/10.1158/0008-5472.CAN-06-0734.
54. Kabrawala, S., Zimmer, M.D., and Campellone, K.G. (2020). WHIMP links the actin nucleation machinery to Src-family kinase signaling during protrusion and motility. PLoS Genet. *16*, e1008694. https://doi.org/10.1371/journal.pgen.1008694.
55. Yamada, H., Padilla-Parra, S., Park, S.-J., Itoh, T., Chaineau, M., Monaldi, I., Cremona, O., Benfenati, F., De Camilli, P., Coppey-Moisan, M., et al. (2009). Dynamic interaction of amphiphysin with N-WASP regulates actin assembly. J. Biol. Chem. *284*, 34244–34256. https://doi.org/10.1074/jbc.M109.064204.
56. Cox, E.A., Bennin, D., Doan, A.T., O'Toole, T., and Huttenlocher, A. (2003). RACK1 Regulates Integrin-mediated Adhesion, Protrusion, and Chemotactic Cell Migration via Its Src-binding Site. Mol. Biol. Cell *14*, 658–669. https://doi.org/10.1091/mbc.E02-03-0142.
57. Buensuceso, C.S., Woodside, D., Huff, J.L., Plopper, G.E., and O'Toole, T.E. (2001). The WD protein Rack1 mediates protein kinase C and integrin-dependent cell migration. J. Cell Sci. *114*, 1691–1698. https://doi.org/10.1242/jcs.114.9.1691.
58. Leung, T., Chen, X.Q., Manser, E., and Lim, L. (1996). The p160 RhoA-binding kinase ROK alpha is a member of a kinase family and is involved in the reorganization of the cytoskeleton. Mol. Cell Biol. *16*, 5313–5327. https://doi.org/10.1128/MCB.16.10.5313.
59. Hotulainen, P., and Lappalainen, P. (2006). Stress fibers are generated by two distinct actin assembly mechanisms in motile cells. J. Cell Biol. *173*, 383–394. https://doi.org/10.1083/jcb.200511093.
60. Cao, X.-X., Xu, J.-D., Xu, J.-W., Liu, X.-L., Cheng, Y.-Y., Li, Q.-Q., Xu, Z.-D., and Liu, X.-P. (2011). RACK1 promotes breast carcinoma migration/metastasis via activation of the RhoA/Rho kinase pathway. Breast Cancer Res. Treat. *126*, 555–563. https://doi.org/10.1007/s10549-010-0955-3.
61. Lafont, F., Tran Van Nhieu, G., Hanada, K., Sansonetti, P., and van der Goot, F.G. (2002). Initial steps of Shigella infection depend on the cholesterol/sphingolipid raft-mediated CD44-IpaB interaction. EMBO J. *21*, 4449–4457. https://doi.org/10.1093/emboj/cdf457.
62. TANG, Y., GARSON, K., LI, L., and VANDERHYDEN, B.C. (2015). Optimization of lentiviral vector production using

polyethylenimine-mediated transfection. Oncol. Lett. *9*, 55–62. https://doi.org/10.3892/ol.2014.2684.

63. Schindelin, J., Arganda-Carreras, I., Frise, E., Kaynig, V., Longair, M., Pietzsch, T., Preibisch, S., Rueden, C., Saalfeld, S., Schmid, B., et al. (2012). Fiji: an open-source platform for biological-image analysis. Nat. Methods *9*, 676–682. https://doi.org/10.1038/nmeth.2019.

64. McLean, D.J., and Skowron Volponi, M.A. (2018). trajr: An R package for characterisation of animal trajectories. Ethology *124*, 440–448. https://doi.org/10.1111/eth.12739.

65. Bubb, M.R., Senderowicz, A.M., Sausville, E.A., Duncan, K.L., and Korn, E.D. (1994). Jasplakinolide, a cytotoxic natural product, induces actin polymerization and competitively inhibits the binding of phalloidin to F-actin. J. Biol. Chem. *269*, 14869–14871. https://doi.org/10.1016/S0021-9258(17)36545-6.

66. Carisey, A., Stroud, M., Tsang, R., and Ballestrem, C. (2011). Fluorescence Recovery After Photobleaching. In Cell Migration: Developmental Methods and Protocols Methods in Molecular Biology, C.M. Wells and M. Parsons, eds. (Humana Press), pp. 387–402. https://doi.org/10.1007/978-1-61779-207-6_26.

67. Ray, K., Bobard, A., Danckaert, A., Paz-Haftel, I., Clair, C., Ehsani, S., Tang, C., Sansonetti, P., Tran, G.V.N., and Enninga, J. (2010). Tracking the dynamic interplay between bacterial and host factors during pathogen-induced vacuole rupture in real time. Cell Microbiol. *12*, 545–556. https://doi.org/10.1111/j.1462-5822.2010.01428.x.

STAR★METHODS

KEY RESOURCES TABLE

REAGENT or RESOURCE	SOURCE	IDENTIFIER
Antibodies		
Mouse monoclonal anti-RACK1	Santa Cruz	Cat. No. sc-17754
Mouse monoclonal anti-Tubulin-HRP	Santa Cruz	Cat. No. sc-8035
Mouse monoclonal anti-Actin-HRP	Santa Cruz	Cat. No. sc-47778
Goat anti-Mouse-HRP	Bio-Rad	Cat. No. 170-5047
Mouse anti-RACK1-Alexa647	Santa Cruz	Cat. No. sc-17754-AF647
Bacterial and virus strains		
Shigella flexneri wild-type strain M90T expressing AfaI adhesin	John R. Rohde	In this study: *Shigella*
S. flexneri M90T expressing dsRED and AfaI	Yuen-Yan Chang	In this study: dsRED-*Shigella*
Δ*IcsA S. flexneri* M90T expressing dsRED and AfaI	John R. Rohde	In this study: Δ*IcsA-Shigella*
Escherichia coli strain DH5-alpha	Thermo Fisher Scientific	Cat. No. 18265017
E. coli strain Stbl3	Thermo Fisher Scientific	Cat. No. C737303
Chemicals, peptides, and recombinant proteins		
Dulbecco's modified Eagle's medium (DMEM)	Wisent	Cat. No. 319-005-CL
Fetal bovine serum (FBS)	Wisent	Cat. No. 080450
HEPES	Gibco	Cat. No. 15630080
0.05% trypsin-EDTA	Wisent	Cat. No.325-042-CL
Tryptic soy broth (TSB)	BD Bacto™	Cat. No. 21182
Congo red	Sigma	Cat. No. C6277
Carbenicillin	Thermo Fisher Scientific	Cat. No. BP26485
Kanamycin	Sigma	Cat. No. K1377-5G
Lysogeny broth (LB)	BioShop	Cat. No. LBL407
Phosphate-Buffered Saline (PBS)	Wisent	Cat. No. 311-010-CL
Puromycin	Gibco	Cat. No. A11138-03
Blasticidin	Gibco	Cat. No. A11139-03
Gentamycin	Sigma	Cat. No. G4918
Polyethyleneimine (PEI)	Sigma	Cat. No. 765090
FuGENE	Promega	Cat. No. E2311
X-tremeGENE	Sigma	Cat. No. 6365779001
FluoroBrite DMEM	Gibco	Cat. No. A1896701
Fibronectin	Sigma	Cat. No. F1141
Paraformaldehyde (PFA)	EM Sciences	Cat. No. 157-8-100
Phalloidin-Alexa555	Invitrogen	Cat. No. A34055
Phalloidin-Alexa647	Invitrogen	Cat. No. A22287
Methocel A4M	Sigma	Cat. No. 94378
Jasplakinolide (Jasp)	Thermo Fisher Scientific	Cat. No. J7473
Critical commercial assays		
BCA Protein Assay Kit	Thermo Fisher Scientific	Cat. No. 23225

(*Continued on next page*)

Continued

REAGENT or RESOURCE	SOURCE	IDENTIFIER
Experimental models: Cell lines		
HeLa	TakaraBio	Cat. No. 631156
CaCo-2	ATCC	Cat. No. HTB-37
HEK-293T cells	ATCC	Cat. No. CRL-3216
Oligonucleotides		
attagtcgacatgactgagcagatgaccc	This study	RACK1_F-SalI
taattctagactagcgtgtgccaatggtca	This study	RACK1_R-XbaI
ccggtaccctgggtgtgtgcaaatactcg agtatttgcacacacccagggtatttttg	This study	shRNA-92_F
aattcaaaaatacccctgggtgtgtgcaaat actcgagtatttgcacacacccagggta	This study	shRNA-92_R
ccggaggatggccaggccatgttatctcg agataacatggcctggccatccttttttg	This study	shRNA-94_F
aattcaaaaaaggatggccaggccatgtt atctcgagataacatggcctggccatcct	This study	shRNA-94_R
ccggcaagctgaagaccaaccacatctc gagatgtggttggtcttcagcttgtttttg	This study	shRNA-95_F
aattcaaaaacaagctgaagaccaacca catctcgagatgtggttggtcttcagcttg	This study	shRNA-95_R
Recombinant DNA		
pEGFP-C1	Clontech	Cat. No. 6084-1
pEGFP-N1	Clontech	Cat. No. 6085-1
pLJM1	Addgene	Cat. No. 91980
pLKO1	Addgene	Cat. No. 10878
pLKO:NS	Addgene	Cat. No. 1864
psPAX2	Addgene	Cat. No. 12260
pMD2.G	Addgene	Cat. No. 12259
pLV-Ftractin-GFP	Roy Duncan, Dalhousie University	N/A
pLV-F-tractin-mCherry	Addgene	Cat. No. 85131
pmOrange-Galectin3	Ray, K. et al.[67]	N/A
pEGFP-Actin	Ray, K. et al.[67]	N/A
pEGFP:GFP-RACK1	This study	N/A
pEGFP:RACK1-GFP	This study	N/A
pLJM1:RACK1	This study	N/A
pLKO: KD-93	This study	N/A
pLKO: KD-94	This study	N/A
pLKO: KD-95	This study	N/A
Software and algorithms		
Fiji (ImageJ, version 2.3.0)	Schindelin, J. et al.[63]	https://fiji.sc/
R package "growthrates" (version 8.2)	N/A	https://cran.r-project.org/web/packages/growthrates/index.html
R package "trajr" (version 1.4.0)	McLean, D. J. & Skowron Volponi, M. A[64]	https://cran.r-project.org/web/packages/trajr/index.html
Zeiss Zen Black software (version 2.3)	N/A	https://www.micro-shop.zeiss.com/en/us/softwarefinder/software-categories/zen-black/zen-black-system/

(*Continued on next page*)

Continued

REAGENT or RESOURCE	SOURCE	IDENTIFIER
BioVoxxel Toolbox: Speckle Inspector plugin (version 2.5.7)	N/A	https://imagej.net/plugins/biovoxxel-toolbox
R package "Frapplot" (version 0.1.3).	N/A	https://cran.r-project.org/web/packages/frapplot/index.html

RESOURCE AVAILABILITY

Lead contact

Further information and requests for resources and reagents should be directed to and will be fulfilled by the lead contact Zhenyu Cheng (zhenyu.cheng@dal.ca).

Materials availability

Plasmids generated in this study are available upon request.

Data and code availability

- Data reported in this paper will be shared by the lead contact upon request
- This paper does not report original code.
- Any additional information required is available from the lead contact upon request.

EXPERIMENTAL MODEL AND STUDY PARTICIPANT DETAILS

Cell lines culture

HeLa (cervical carcinoma), CaCo-2 (male colorectal adenocarcinoma) and HEK-293T (female embryonic kidney) cells were grown in DMEM supplemented with 10% HI-FBS and 1% HEPES at 37°C with 5% CO_2. Cells were passaged before reaching 100% confluency by adding 0.5 mL of 0.05% trypsin-EDTA to T-25 flasks incubating at 37°C until cells were dislodged from the flask. Cell suspensions were subsequently diluted to the desired cell density.

Shigella strains culture

S. flexneri wild-type strain M90T expressing AfaI adhesin (*Shigella*), M90T expressing dsRED and AfaI (dsRED-*Shigella*), and a Δ*IcsA* mutant strain expressing dsRED and AfaI (Δ*IcsA*-*Shigella*) were used in this study. The *E. coli*-derived afaI gene confers *Shigella* with much higher invasion capabilities, which is desirable for time-lapse imaging.[61] *Shigella* strains were grown in tryptic soy broth (TSB) supplemented with 15 g/L agar, 100 μg/mL carbenicillin and 0.02% (w/v) Congo red to select for functional T3SS system (red colonies). Inoculated TSB plates were incubated for 15 to 20 h at 37°C.

For infection experiments, *Shigella* were grown overnight (ON) in TSB, supplemented with carbenicillin (100 μg/ml), at 37°C with shaking at 200 rpm. The next day, bacteria were diluted to 1/100 dilution in fresh TSB with carbenicillin (100 μg/ml) and incubated for 2.5 hrs to an optical density at 600 nm (OD_{600}) between 0.4 to 0.6 (exponential growth phase). To prepare the inoculum, 1 mL of exponential *Shigella* growth culture was washed once with PBS by centrifuging at 5000 x g for 1 min; then, the culture was resuspended in serum-free DMEM to the desired multiplicity of infection (MOI).

METHOD DETAILS

Recombinant DNA and lentiviral transduction

The RACK1 gene was amplified from HeLa cDNA using primers RACK1_F-SalI and RACK1_R-XbaI and cloned into pEGFP-C1 and pEGFP-N1 to obtain pEGFP:GFP-RACK1 and pEGFP:RACK1-GFP, respectively. An untagged version of RACK1 was constructed by subcloning the RACK1 gene from pEGFP-C1-RACK1 without the GFP gene into pLJM1, generating pLJM1:RACK1. RACK1 expression was silenced in HeLa and CaCo-2 cells using shRNAs targeting three regions of the RACK1 mRNA (NM_006098.4). The shRNAs oligos were annealed and cloned into the pLKO1 vector to generate pLKO: KD-93, pLKO: KD-94 and pLKO: KD-95. A pLKO:NS plasmid carrying scrambled RNA was used as the negative control. Lentivirus particles carrying the silencing plasmids were produced in HEK-293T cells by co-transfecting the pLKO constructs, psPAX2 packaging plasmid and pMD2.G envelope plasmid with 1 mg/mL of PEI, as previously described.[62] Lentiviruses carrying pLJM1-RACK1, pLV-F-tractin-GFP, and pLV-F-tractin-mCherry were generated using this protocol. The lentiviral particles were subsequently used to transduce HeLa or CaCo-2 cells, generating stable RACK1-KD cell lines and fluorescent reporter cell lines. Puromycin (1 μg/mL) or blasticidin (4 μg/mL) were used to select cells that stably express the transduced constructs.

RACK1 expression assessment by western blotting

HeLa or CaCo-2 cells transduced with lentiviruses carrying silencing shRNAs were harvested by trypsinization, washed twice in PBS, and re-suspended in 400 µl of lysis buffer (2% SDS w/v, 50mM Tris/HCl pH 7.4). Lysates were boiled at 95°C for 5 min and sonicated at 25 watts for 30 sec. Debris was removed by centrifugation at 14000 x g for 10 min at four °C. Ten µg of these whole-cell lysates were separated on a 12% SDS polyacrylamide gel. Proteins were then transferred to a 0.2 µm PVDF membrane, blocked with 5% non-fat milk, immunoblotted with anti-RACK1 (1/1000), followed by anti-mouse-HRP (1/10000). Anti-Tubulin-HRP (1/5000) and Anti-Actin-HRP (1/5000) were loading controls. Quantitative analyses were performed using Fiji (ImageJ) software,[63] measuring the RACK1 band intensity and normalizing it by the corresponding tubulin band intensity.

Gentamycin protection assay to measure intracellular *Shigella* growth

Target cells (2.5 x10^5 cells/well) were seeded in 12-well plates. The following day, the cells were infected for 30 min at 37°C with 1 mL/well of *Shigella* inoculum at the desired MOI. Following a wash with PBS, the monolayers were treated for 15 min with DMEM supplemented with gentamycin (100 µg/mL) to eliminate extracellular bacteria. After three washes with PBS, the cells were lysed (time-points: 0, 1, 2 and 3 hrs post gentamycin treatment) with 200 µL of NP-40 buffer (0.1% NP40, 50 mM Tris-HCl pH 7.5, 5 mM EDTA, 10% glycerol, 100 mM NaCl) for 5 min. The lysates were then serially diluted, inoculated into LB agar plates and incubated overnight at 37°C. Colony Forming Units (CFUs) were counted and normalized by the total protein concentration (determined by BCA kit) on each well to account for cell number variability due to losses during washes. *Shigella* growth rates on each cell line were calculated using the grow_logistic function from the R package "growthrates" (version 8.2).

Time-lapse confocal microscopy of *Shigella* invasion

To evaluate RACK1 recruitment to *Shigella*'s entry focus, HeLa cells (1x10^5 cell/well) stably expressing RACK1-GFP and F-tractin-mCherry were seeded on 4-well 35 mm glass-bottom dishes. After 24 hrs, the cells were infected with *Shigella* (MOI 50) and imaged every 1 min for 1.5 hrs with a 63X objective on a Zeiss spinning disk microscope. We used a galectin-3 reporter to study the role of RACK1 during the *Shigella* invasion of epithelial cells and vacuolar escape. For this experiment, 6 x 10^3 cells/well of KD-92 and NS HeLa were seeded on black 96-well plates and transfected with pmOrange-Galectin3 (vacuolar rupture reporter[31,67]) and pEGFP-Actin following FuGENE's manufacturer instructions. After 48 h, the cell media was replaced by 50 µL of FluoroBrite DMEM(imaging medium). Infection was performed by adding 50 µL of *Shigella* inoculum (MOI 10) before image capture. Cells were imaged every 1 minute for 1.5 hrs at 37°C and 5% CO_2 using the widefield microscope Nikon Eclipse Ti with 40X magnification. The number of infected cells was calculated by identifying HeLa cells with at least one Gal-3 positive (Gal-3+) signal. Similarly, the number of Gal-3+ bacteria per cell was manually enumerated.

To analyze vacuolar escape, we manually noted the time of *Shigella* entry, defined as the time (in the video) where the first signs of actin cytoskeleton reorganization induced by *Shigella* could be recognized (F-actin-GFP enrichment). After bacterial invasion, the recruitment of Gal-3 to the damaged SCV marked the time of vacuolar escape. These time points were used to calculate the vacuolar escape time in control and RACK1-KD cells as follows: Gal-3+ time minus entry time = escape time.

To evaluate entry foci dynamics, NS and KD-92 HeLa cells stably expressing F-tractin-GFP were infected with dsRED-*Shigella* (MOI 10). Z-stack images (4 slices, 1.2 µm apart) were captured every 2 min with a 63X objective on a Zeiss spinning disk microscope. Average projections of the top 4 slices were generated using Fiji software. Entry foci were identified by increasing F-actin recruitment around dsRED-*Shigella* over time. The largest area reached by entry foci was encircled to create regions of interest (ROIs) from which the area and FI were measured, starting from the first signs of actin recruitment until the FI returned to the basal level. The duration of each focus was calculated by multiplying the number of time points by 2 min (frame acquisition time). The FI data was used to calculate the rate of actin recruitment to the entry foci using the R package "growthrates" (version 8.2). We repurposed the grow_logistic function from this package to estimate the actin's maximum recruitment rate (mumax) using the FI increment over time observed on each infection focus. The model's fitting of the FI curves was visually verified, and curves not well described by the model were eliminated from the final data set.

Primary infection evaluation

The Δ*IcsA Shigella* strain cannot spread from cell to cell due to a lack of actin tail polymerization reflecting the number of primary infected cells. For this experiment, 2.5 x 10^4 RACK1-KD or NS control HeLa cells stably expressing F-tractin-GFP were seeded on black 96-well plate wells. After 24 hrs, the cells were infected with 100 µL of Δ*IcsA Shigella* (OD600 = 0.5 diluted 1/100). The infection was carried out for 30 min at 37°C with 5% CO2, followed by 15 min of gentamycin (100 µg/mL) treatment. After this time, the cells were washed with PBS, and 100 µL of FluoroBrite was added to each well and incubated for 4 hrs. Images were captured using a Zeiss Axio Observer Z.1 widefield microscope at 10X magnification. Cells with one or more intracellular bacteria were considered infected.

Immunofluorescence of infected epithelial cells for actin tail evaluation

For RACK1 localization, 2.5 × 10^5 HeLa cells stably expressing F-tractin-GFP were seeded on 12 mm round glass coverslips pretreated with 20 µg/mL of fibronectin. The cells were infected with dsRED-*Shigella* MOI of 10 for 30 min at 37°C with 5% CO2, followed by treatment with gentamycin (100 µg/mL) for 15 min. The cells were washed with PBS, and fresh DMEM was added before continuing the infection for two more

hours to allow actin tail polymerization. After infection, the cells were fixed with 4% paraformaldehyde for 20 min and immunolabeled with anti-RACK1-Alexa647 (1/100) and phalloidin-Alexa555 (1/100).

For actin tail counting, shape, and FI measurements, 2.5 × 10^5 KD-92 and NS HeLa or CaCo-2 cells seeded on glass coverslips were infected with dsRED-*Shigella* (MOI 10) for three hrs, fixed and stained with phalloidin-Alexa647 (1/100). Z-stacks (6 slices, 1.2 μm) were acquired at 63X magnification on a confocal Zeiss 880. Average projections of the top 4 slices were generated using Fiji. Bacteria with and without actin tails were manually enumerated. Fiji's polygon selection tool was used to manually define ROIs around tails formed in HeLa cells. These ROIs were then used to measure Feret's diameter and FI of the tails.

Time-lapse confocal microscopy of *Shigella* actin-mediated motility

For live observation of *Shigella* trajectories, 1x10^5 F-tractin-GFP HeLa cells (KD-92 and NS) were seeded in 4-well 35 mm glass-bottom dishes. A day after, the cells' medium was replaced with 450 μL of FluoroBrite, and the infection was carried out by adding 50 μL of dsRED-*Shigella* (OD_{600} = 0.5 culture diluted 1 in 10 with PBS). Z-stacks (5 slices, one μm) images were captured at 63X magnification every 60 sec for two hrs at 37°C and 5% CO2 using a Zeiss Axio Observer Z.1 spinning disk microscope. The z-stacks time-lapse images were transformed into average intensity projections without the first 2 (bottom) slices of the z-stack to avoid stress fibre interference. Then, bacterial movements were recorded using Fiji's Manual Tracking tool for as long as the bacterium was visible and stopped if the bacterium divided, went out of the focal plane or stoped for more than 5 frames. The distance between every two points in each trajectory was calculated as d =√((x2-x1)^2+(y2-y1)^2). Trajectory speed, sinuosity index and tumbling analysis were characterized using the "trajr" (version 1.4.0)[64] package in R.

Evaluation of *Shigella* cell-to-cell spreading via plaque assay

F-tractin-GFP HeLa and GFP-CaCo-2 cells were seeded in black 96-well plates and grown to confluence. The monolayers were subsequently infected with a diluted culture of dsRED-*Shigella* (OD_{600} = 0.5 diluted 1000 times) for 30 min before incubation with gentamycin (100 ug/mL) for 15 min. Then the cells were overlaid with 100 μL 0.4% Methocel A4M (Sigma) diluted in FluoroBrite DMEM. Infections were carried out at 37°C with 5% CO2 for 10 (HeLa) or 15 (CaCo-2) hrs before imaging at 10X magnification using a Zeiss Axio Observer Z.1 widefield microscope. To image around 50% of the well's area, 16 tiles were captured and stitched using Zeiss Zen Black software (version 2.3). *Shigella* plaques' area was measured by automatic segmentation using Fiji. Briefly, the images were separated into two channels (GFP = cells, dsRED = bacteria), and the background was subtracted from the dsRED channel images (rolling = 90). Then, the filters *Median* (radius = 10) and *Gaussian blur* (sigma = 10) were applied before transforming the images into masks using the *Mean thresholding* method with default settings. The commands *Dilate mask* and *Fill Holes* further defined the plaques contour. The final mask images were input to the *Analyze particles* (size = 0.1 to infinity) tool to identify the plaque's outlines.

To assess *Shigella* cell-to-cell spreading using high magnification time-lapse images, 1 x 10^5 F-tractin-GFP HeLa cells (NS and KD-92) were seeded in 4-well glass-bottom dishes. The next day, cells were overlaid with 0.4% Methocel and infected with eight μl of dsRED-*Shigella* (OD_{600} = 0.5 diluted 1000 times). Infection foci, comprised of 1 infected HeLa cell, were located using the eyepiece of the microscope. Then, 9-tile images were captured at 40X magnification every 15 min for 15 hrs at 37°C and 5 % CO2 on a Zeiss Axio Observer Z.1 spinning disk. *Shigella* cell-to-cell spreading was quantified by recording the number of infected cells at each time point. The spreading rate of *Shigella* was calculated from the log-linear part of the spreading curve using the all_splines function from the R package "growthrates" (version 8.2).

Evaluation of actin polymerization in uninfected cells

Jasplakinolide (Jasp) induces actin filament stabilization leading to G-actin polymerization into amorphous F-actin aggregates.[65] Before treatment, NS and KD-92 HeLa cells stably expressing F-tractin-GFP were seeded in 4-well glass-bottom dishes (1x10^5 cells/well). After 24 h, the medium was substituted with 300 μl of FluoroBrite and incubated for 15 min in the microscope's atmosphere-regulated chamber (37°C, 5% CO2) to stabilize the cells. Then, 200 μl of 0.5 μM Jasp diluted in FluoroBrite was added to each well. Z-stack images (8 slices, 1μm apart) were captured before adding Jasp and after two hrs using a Zeiss Axio Observer Z.1 spinning disk microscope with 40X magnification. The F-actin aggregates formed were automatically segmented and analyzed using Fiji's Speckle Inspector plugin from the BioVoxxel Toolbox (version 2.5.7).

FRAP was carried out following a protocol described by Carisey et al.[66] to analyze actin turnover in stress fibres and membrane ruffles of uninfected cells. Briefly, 5x10^4 NS and KD-92 HeLa cells were seeded in 4-well glass-bottom dishes and transfected with pEGFP-Actin[67] following X-tremeGENE manufacturer instructions. After 48 h, the medium was replaced with FluoroBrite. One hour before imaging, dishes were placed in the microscope's atmosphere-regulated chamber (37°C with 5% CO2) to allow the medium to equilibrate. A Zeiss LSM 880 confocal microscope was used to capture 16-bit, 512 x 512 pixels images at 63X magnification using bi-directional scanning at speed 7. The pinhole size was set to 1 Airy Unit, and the zoom factor was 2. The power of the 488 nm argon laser was set to 22% (gain: 652, offset: 62) during imaging and increased to 100% for the bleaching pulses on a rectangular ROI. Three images were captured before bleaching within the ROI for two iterations. Images continued to be captured every 2 sec for 172 sec after bleach. Stress fibres and ruffles were analyzed in 25 NS and 22 KD-92 cells. Fluorescence recovery curves were analyzed using the R package "Frapplot" (version 0.1.3).

QUANTIFICATION AND STATISTICAL ANALYSIS

Statistical differences between control and RACK1 silenced conditions were performed using R. Appropriated tests were chosen according to the data distribution, normality, and hypothesis testing and are indicated on each figure legend. The normality of the data was tested using Shapiro-Wilk's method. Independent t-test (normal distribution) and Wilcoxon rank-sum test (not normal distribution) were used for two-condition experiments. ANOVA (normal distribution) followed by posthoc TukeyHSD test and Kruskal-Wallis (not normal distribution) followed by Dunn's test were used to evaluate statistical differences in experiments with more than two conditions. Statistical significance was reported as follows: ns = not significant; *p <0.05; **p < 0.01; ***p < 0.001, and ****p <0.0001. Only statistically significant differences are labelled in figures.